Particle image velocimetry measurements of flow around an escort tug model with a yaw angle of 45 degrees

Molyneux, D.

Publisher's version / Version de l'éditeur:
https://doi.org/10.4224/8895077
Technical Report(National Research Council of Canada. Institute for Ocean Technology); no. TR-2006-18, 2006

DOCUMENTATION PAGE

REPORT NUMBER	NRC REPORT NUMBER	DATE
TR-2006-18		July 2006
REPORT SECURITY CLASSIFICATION		**DISTRIBUTION**
Unclassified		Unlimited

TITLE

PARTICLE IMAGE VELOCIMETRY MEASUREMENTS OF FLOW AROUND AN ESCORT TUG MODEL WITH A YAW ANGLE OF 45 DEGREES

AUTHOR(S)

David Molyneux

CORPORATE AUTHOR(S)/PERFORMING AGENCY(S)

Institute for Ocean Technology, National Research Council, St. John's, NL

PUBLICATION

SPONSORING AGENCY(S)

Institute for Ocean Technology, National Research Council, St. John's, NL

IOT PROJECT NUMBER	NRC FILE NUMBER
42_2072_10	

KEY WORDS	PAGES	FIGS.	TABLES
escort tug, Particle Image Velocimetry (PIV), flow patterns	iii, 42, App. 1	34	4

SUMMARY

This report describes model experiments carried out to measure the flow patterns around a scale model of an escort tug using Particle Image Velocimetry (PIV). The PIV system is described in detail elsewhere (Molyneux, 2006). This report describes the experiment methods and presents the results. Some discussion on the results is given and recommendations for improvements to the experiment techniques are made.

ADDRESS National Research Council
Institute for Ocean Technology
Arctic Avenue, P. O. Box 12093
St. John's, NL A1B 3T5
Tel.: (709) 772-5185, Fax: (709) 772-2462

National Research Council Canada
Institute for Ocean Technology

Conseil national de recherches Canada
Institut des technologies océaniques

PARTICLE IMAGE VELOCIMETRY MEASUREMENTS OF FLOW AROUND AN ESCORT TUG MODEL WITH A YAW ANGLE OF 45 DEGREES

TR-2006-18

David Molyneux

July 2006

TABLE OF CONTENTS

LIST OF TABLES

LIST OF FIGURES

LIST OF FIGURES (cont'd)

PARTICLE IMAGE VELOCIMETRY MEASUREMENTS OF FLOW AROUND AN ESCORT TUG MODEL WITH A YAW ANGLE OF 45 DEGREES

1.0 INTRODUCTION

One of the main design requirements of an escort tug is that it must operate at speeds up to 10 knots, with a yaw angle between 35 and 55 degrees. In this condition the hull generates a large hydrodynamic force, which is used to turn a disabled tanker. A significant feature of an escort tug design is the large, low aspect ratio fin at the bow, which is not common on other types of ship. This fin generates 50 percent of the total hydrodynamic force at the operating yaw angles, and so it is expected that it will have a large effect on the flow patterns around the tug.

Preliminary experiments were carried out to develop some of the techniques necessary for obtaining reliable results from PIV measurements for a hull with a yaw angle in a towing tank (Molyneux & Xu, 2005). This work included the development of a prototype seeding system and finding the most suitable orientation of the laser sheet relative to the direction of motion of the hull. Some preliminary predictions of the flow patterns for a yaw angle of 45 degrees, with and without the fin were made using *Fluent*, a commercial computational fluid dynamics program (Molyneux, 2005) and the results of these simulations were used to plan the experiments described in this report.

The preliminary CFD simulations had shown that the effect of the fin was most visible on the flow patterns under the hull, on the downstream side of the centreline. This region of the flow should contain a large vortex formed by the fin. In order to visualize this large vortex, the laser plane for the PIV system needed to be oriented across the direction of the undisturbed flow.

This report describes model experiments carried out to measure the flow patterns around a scale model of an escort tug using Particle Image Velocimetry (PIV). The PIV system is described in detail elsewhere (Molyneux, 2006). This report describes the experiment methods and presents the results. Some discussion on the results is given and recommendations for improvements to the experiment techniques are made.

2.0 DESCRIPTION OF SHIP MODEL

The hull chosen for the flow measurements was a concept for a tractor tug developed by Robert Allan Ltd. of Vancouver, B. C (Allan & Molyneux, 2004). The 1:18 scale model was previously tested at the NRC Institute for Ocean Technology (IOT). During these experiments, measurements were made of the lift and drag forces for the hull in combination with different appendages over a range of ship speeds from 4 to 12 knots (with model speeds based on Froude scaling), for yaw angles between zero and 105 degrees (Molyneux, 2003). During these initial experiments the hull was free to heel,

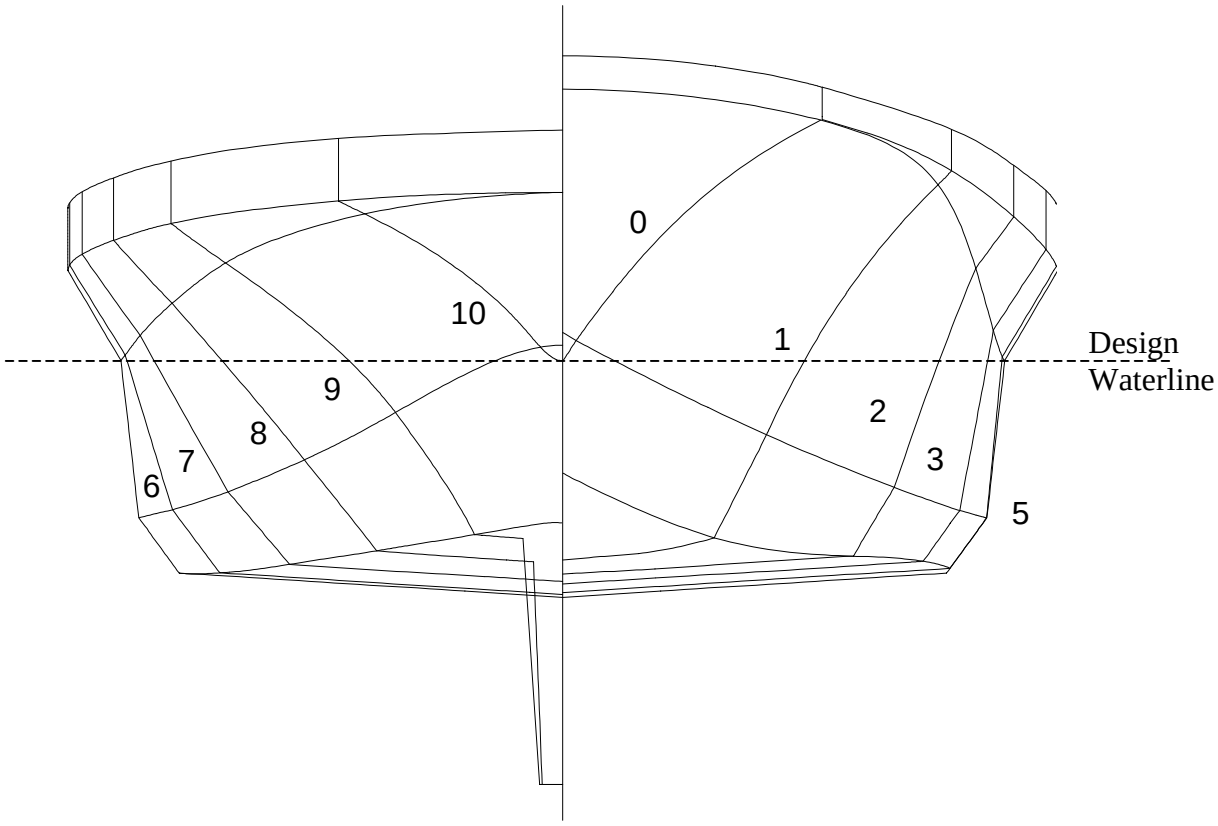

Figure 1, Body plan for tug model, used in PIV experiments

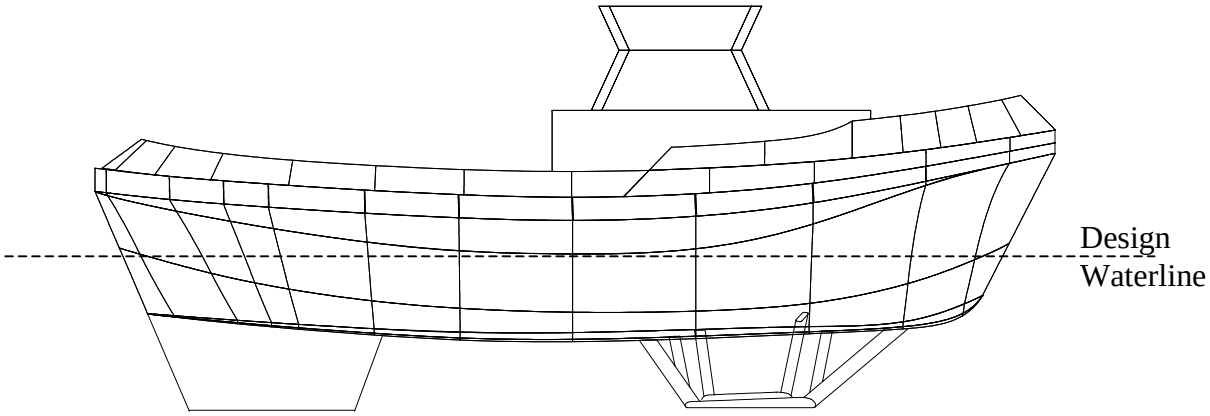

Figure 2, Profile view of tug, with fin and propulsion cage

sink and trim. The body plan for the tug is shown in Figure 1 and the profile is shown in Figure 2. A summary of the tug geometry is given in Table 1. For this series of experiments the model was always moving with the fin (when fitted) going forwards (although the ship is actually going astern based on conventional definitions of bow and stern).

Length, waterline, m	2.122
Beam, waterline, m	0.789
Draft, hull, m	0.211
Daft, maximum, m	0.471
Displacement, kg	213.3
Nominal scale	1:18

Table 1, Summary of model particulars

To reduce the corruption of recorded images by reflected laser light, the hull was painted matt black. Contrasting targets, made from narrow yellow strips of tape were placed at key locations on the model. These were used to align the laser beam, to ensure that it was at the required position relative to the model.

For the PIV experiments no bulwarks or deckhouses were fitted, although they are shown in the figure. The propulsion cage was also removed, so that the fin was the only appendage. Some experiments were also carried out with the fin removed.

3.0 PROGRAM OF EXPERIMENTS

3.1 Test Conditions

The yaw angles and speeds for which PIV measurements were made are summarized in Table 2. The mean yaw angle for escort tug operation is 45 degrees. Two speeds were chosen to cover the expected range of operation for the ship.

Yaw angle, degrees	Model speed, m/s	Ship speed, knots
45	0.5	4.12
45	1.0	8.24

Table 2, Yaw angles and speeds tested

Preliminary CFD simulations (Molyneux, 2005) had shown that the fin had a very large effect on the flow patterns on the underside of the hull and on the downstream side. To confirm this prediction, some experiments were carried out with the fin removed. The

CFD predictions also indicated that the fin had a very small effect on the upstream side and so experiments for that location were only carried out with the fin removed.

The preliminary test plan called for multiple yaw angles for the tug and multiple sections along the hull at each yaw angle. Not all of these measurements could be obtained, for reasons that will be discussed later in the report. The final measurement plane locations and the appendage configurations are given in Table 3.

Measurement location	Yaw angle, degrees	Appendages	Speed, m/s
Midships, upstream side	+45	Fin off	0.5, 1.0
Midships, downstream side	-45	Fin off	0.5, 1.0
Midships, downstream side	-45	Fin on	0.5, 1.0

Table 3, Summary of measurement plane locations

3.2 Installation of Model and PIV System in IOT's Ice Tank

The preliminary CFD simulations (Molyneux, 2005) predicted that more than one measurement window from the PIV system was required to fully observe the flow patterns caused by the fin. The disturbance to the flow by the fin was expected to cover an area of approximately 1.0m by 0.5m on the downstream side of the hull. A typical measurement window for the PIV system was 0.3m square. If the PIV system had to be moved to obtain this range of measurement, there was the potential requirement to recalibrate the system each time it was moved. It was important not to waste facility time, which was limited, and so the test set-up was designed to allow the laser to remain fixed in one location. Movement of the measurement window relative to the model was obtained by moving the model or by moving the complete PIV system as a unit.

The laser sheet was oriented across the tank, normal to the direction of motion of the towing carriage. A flow-based coordinate system was chosen, since this would eliminate the need to re-orient the laser plane for each change of yaw angle of the tug.

The sign convention for the model geometry (used for the CFD simulations) was a right-handed system, with the origin at the leading edge of the static waterline (the end of the hull with the fin), x positive from the bow to the stern, and z positive upwards. On this coordinate system, the yaw angle was positive when the bow was turned to port. Note that for the upstream side, the yaw angle was changed to 45 degrees, so that the PIV system did not have to be moved.

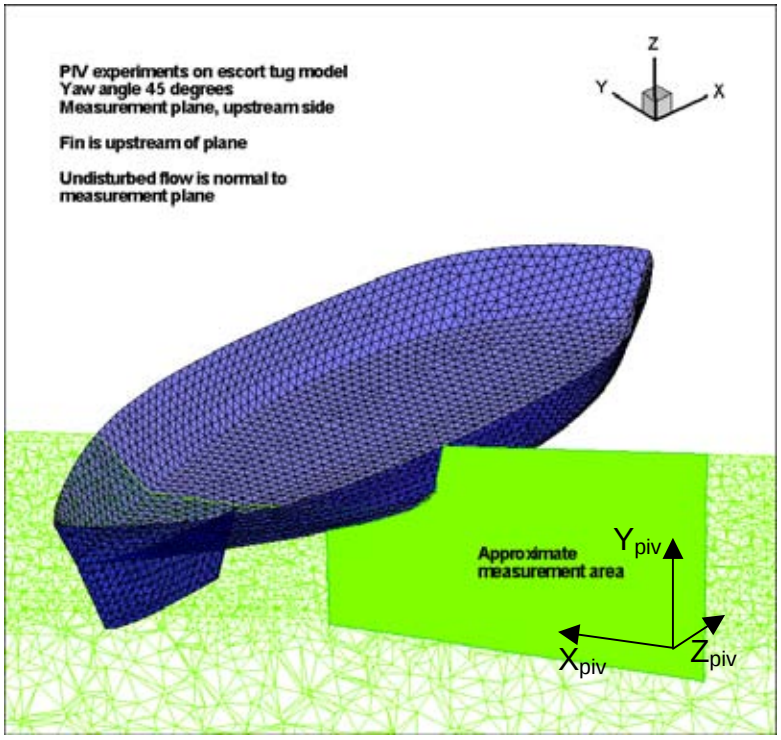

Figure 3, Location of measurement plane, upstream side of hull

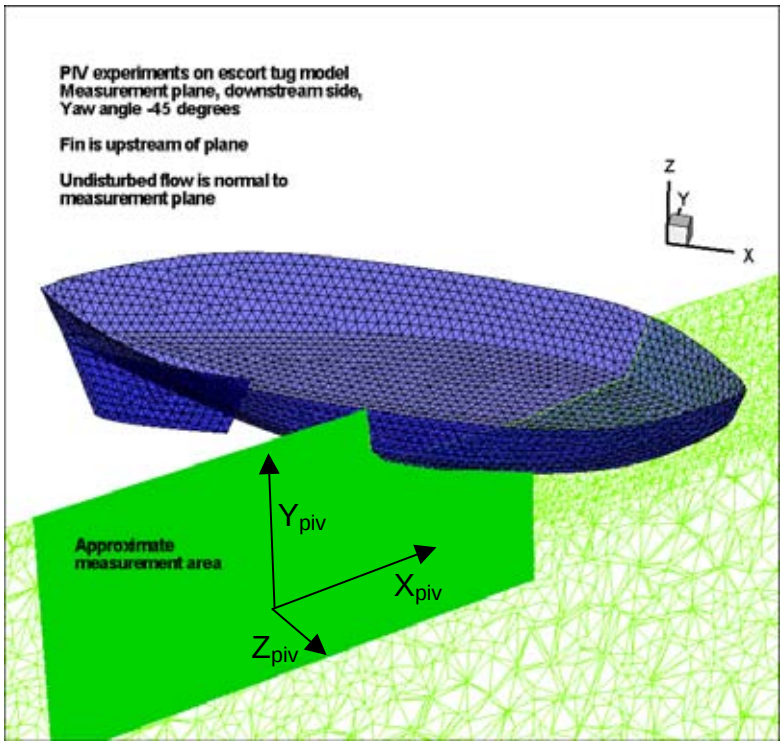

Figure 4, Location of measurement plane, downstream side of hull

The results of the PIV experiments given below are presented using a coordinate system, which was based on the measurement plane (LaVision, 2005). In this system, *x* and *y* axes were within the measurement plane, and the *z* axis was through the measurement plane. The measurement planes relative to the model geometry and the coordinate systems are shown in Figure 3 for the upstream side and Figure 4 for the downstream side. In the PIV coordinate system, undisturbed flow had a *z* velocity component, equal to the speed of the towing carriage, and the *x* and *y* velocity components would be zero.

The PIV measurements were carried out in the Ice Tank of the National Research Council's Institute for Ocean Technology. In the centre of the carriage was a test frame, which was adjustable vertically and had two longitudinal beams that can be moved independently but remain parallel to the centreline of the carriage. This adjustment feature was used to vary the location of the measurement window, relative to the model. Each beam had a scale so that the exact locations of the beam, relative to the centreline of the test frame were known. The PIV equipment was fitted to the beam on the South side of the carriage, and the model was fitted to the beam on the North.

At a given yaw angle and measurement section, the most common movement of the measurement window was in the *x*-direction of the PIV axis. This was obtained by moving one or other of the test beams. Vertical movement (*y*-axis in the PIV system) was the next most frequent adjustment, which was made by raising or lowering the borescopes and laser fixed amounts. The model and attachment frame were moved along the test beam until the target at the required section was aligned with the laser sheet. Once this was obtained, the model was clamped in place. Yaw angle was the least frequent adjustment, and this was made using a yaw table, built for earlier model tests on an Autonomous Underwater Vehicle.

A frame for the PIV system was built around one test beam, using extruded aluminium sections. The laser was oriented normal to the direction of motion, so that the measurement plane was across the direction of motion for the undisturbed flow. The borescopes for the CCD cameras were mounted symmetrically, approximately 650mm either side of the laser sheet. Camera 1 was upstream of the laser sheet, and Camera 2 was downstream. The centre of the measurement window was approximately 950 mm away from the under the water optical unit for the laser. At no time during the testing were these positions changed. The minimum separation between the beams of the test frame was 922 mm. The final arrangement of the PIV system on the Ice Tank carriage test beam is shown in Figure 5.

The model was connected to the carriage by two vertical, cylindrical poles and a yaw table. This yaw table enabled yaw angle to be adjusted from zero to ninety degrees, in five-degree increments. The model hull was rigidly connected to the towing carriage, by bolting the yaw table around the carriage beam. Yaw angle for the model was adjusted using the yaw table. To adjust the position of the model, relative to the laser sheet, the bolts around the beam were slacked off and the model slid forwards or backwards as required until the laser sheet was directed at the correct target on the model. The model and the assembled PIV system are shown in Figure 6.

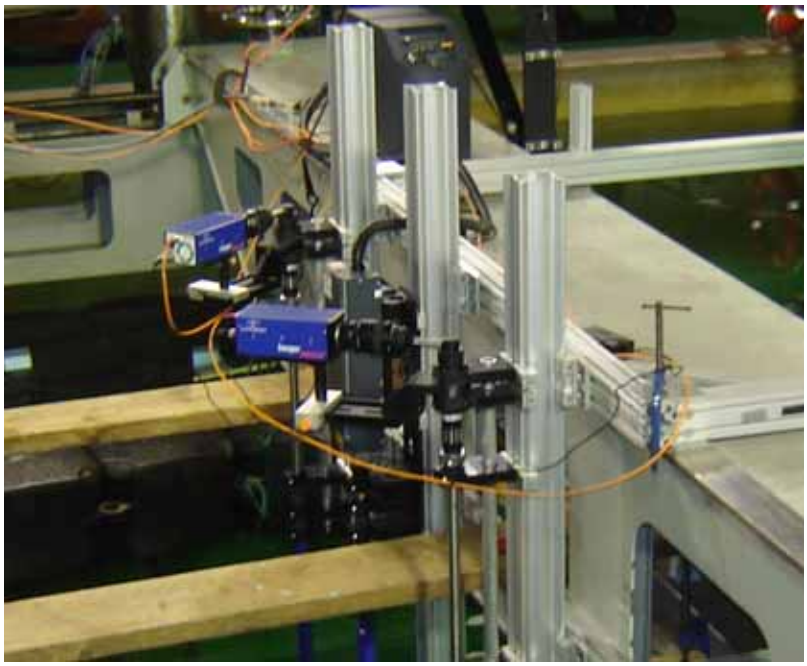

Figure 5, PIV system attached to towing carriage in IOT Ice Tank

Figure 6, Escort tug model and PIV system attached to towing carriage in IOT Ice Tank (model shown at zero yaw angle)

3.3 PIV System Calibration, Operation and Maintenance

In-situ calibration of the measurement space was carried out prior to testing using a Type 30 calibration plate, supplied by LaVision GmbH. The plate was suspended from the model using an adjustable support frame. During calibration, the top of the plate was level with the waterline. The plate was adjusted, using the frame, until it was aligned with the laser sheet. Figure 7 shows the calibration plate and the laser.

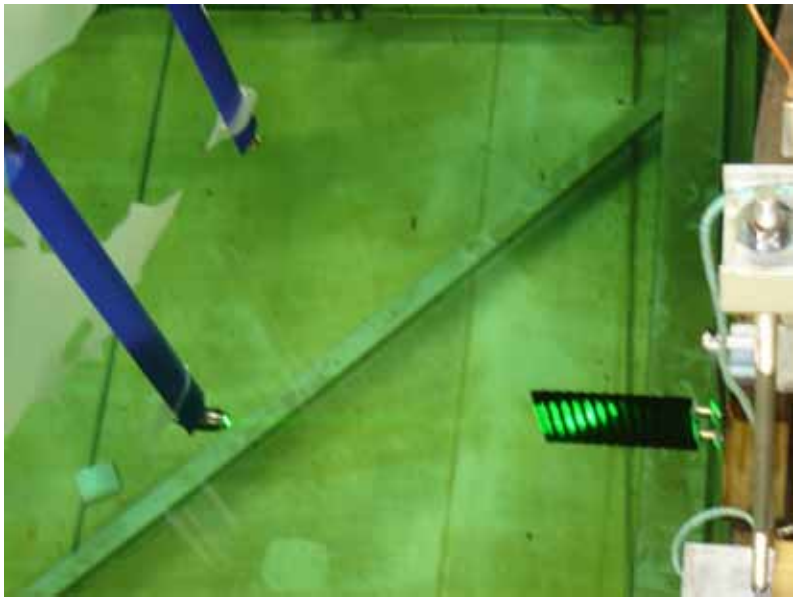

Figure 7, Calibration plate location for in-situ calibration of measurement space

The calibration was carried out using visible light, following the procedures required in the DaVis 7.1 software (LaVision, 2005). Although the system was not moved, it was recalibrated once during the middle of the testing. The PIV system, including the expected uncertainties, has been described in detail (Molyneux, 2006).

The summary of the fit of the mapping function to the known grid points and the resulting size of the de-warped image is given in Table 4.

Date	RMS Deviation Camera 1	RMS Deviation Camera 2	De-warped window size, Pixels (*x*-*y*)	De-warped window size, mm (*x*-*y*)
1st calibration January 13, 2006	0.16625	0.12142	2367 x 1258	525.03 x 273.34
2nd calibration January 20, 2006	0.30769	0.13965	2128 x 1228	438.74 x 249.79

Table 4, Summary of mapping function fit to known grid points

The reference frame for analysis of the images was a right-handed axis system for *x*, *y* and *z* velocity components. The *x*-*y* plane was in the plane of the laser sheet, with the *x*-axis parallel to the water surface. Positive *x* was from port to starboard on the ship model, and positive *y* was towards the water surface. The *z*-axis was positive in the direction of the carriage motion.

On completion of the calibration, the position of the beams was adjusted until the edge of the model at the upper borescope location was clearly visible in the camera images. This position was then used as the reference location. Since more than one view of the flow patterns was required, the relative position of the model and the laser were adjusted from this origin, by moving one or the other of the test beams. Moving the model away from the laser was a negative shift in the *x*-direction, and moving the laser nearer the model was a positive shift, based on the coordinates used for the PIV measurements.

The same general procedure for the carrying out the experiments was followed throughout the test program. First the model or the laser was adjusted to the required position, by moving one of the test beams. The most appropriate seeding rake was selected and its best location for each experiment was found by trial and error. During these trial runs, the optimum time interval for the exposures was also determined. Once the best seed particle distribution and timing had been determined, images were collected for 50 or 100 successive time intervals for speeds of 0.5 and 1.0 m/s, with at least one repeat run for each condition.

For each data collection run, the sequence of action was to turn on the seeding system as the carriage started to move. PIV image data was collected for 50 or 100 image pairs once the carriage had reached a steady speed. On completion of data collection, the carriage was stopped and returned to its initial position. All runs were made collecting data when the carriage was moving towards the melt pit (from East to West). On completion of all the data collection runs at one location, the beam with the model or the beam with the laser was moved to the new position. A summary of all the experiments, including test dates, measurement locations, number of image pairs used in analysis and the time intervals between the laser pulses, is given in Appendix 1.

Some routine checks were performed throughout the test program. Prior to the start of testing each day, the focus of each camera was checked. This was done by seeding the measurement space when the carriage was stationary and if necessary, adjusting the focus of the borescopes. In order to keep the PIV system optics clean, the borescopes and the laser tube were raised out of the water at the end of each day's testing. The optical parts were then washed with fresh water and lens cleaner to prevent the build-up of dirt.

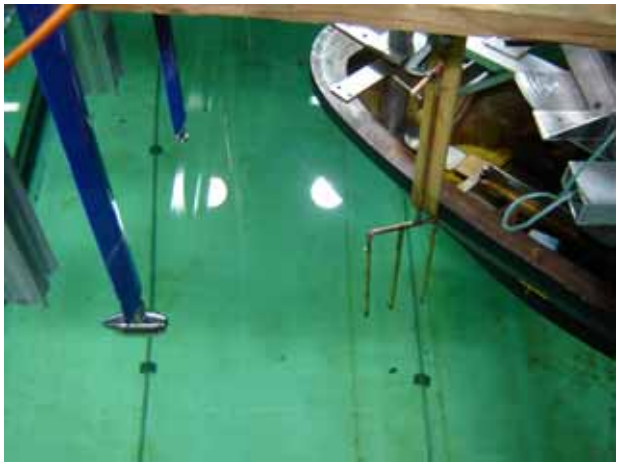

Figure 8(a), Seeding location close to hull and free surface

Figure 8(b), Seeding location close to hull but below free surface

Figure 8(c), Seeding location far from hull

3.4 Seeding

Seeding the flow proved to be the most challenging aspect of carrying out these experiments. The CFD predictions suggested that the most important flow patterns were caused by the fin, and occurred under the hull towards the downstream side. For regions close to the hull, the three-fingered vertical rake was used. A typical installation is shown in Figure 8(a). The flow in this region was unsteady, with quite abrupt changes in direction. As a result, locating the seeding rake was largely a matter of trial and error. The final location of the seeding rake for each measurement window had to be far enough upstream that the wake from the rake has stabilized, but close enough that the required concentration of particles was obtained across a large enough part of the measurement window. This position varied depending on the flow conditions and the location of the measurement window relative to the tug.

For locations close to the hull surface, but below the free surface the 3-fingered horizontal rake was used. The shape of this rake allowed it to get well under the model. This rake could be used for seeding from the upstream or downstream side of the model. Upstream seeding was used when the measurement window was under the hull, and close to the centreline of the hull. Downstream seeding was used when the measurement window was on the downstream side of the hull at the deepest locations for the measurement window. A typical location for seeding on the downstream side of the model is shown in Figure 8(b).

As the measurement window was moved to be far away from the model, the type of rake chosen was less critical. Any of the rakes could be used for measurements in these regions, and Figure 8(c) shows the 3-fingered horizontal rake located for seeding a measurement area well away from the model.

Some representative pictures of the seed particles, at a location close to the model are shown in Figures 9(a) and 9(b). Figure 9(a) shows the view from Camera 1 and Figure 9(b) shows the view at the same time from Camera 2. These pictures were obtained from Run 15:29:35[1], recorded on January 18, 2006 and were chosen because they show the degree of overlap of the two fields of view, relative to a section of the model. The bright line in each figure is the laser shining on the hull, and shows the model from the waterline to the corner of the bilge. The seeding rake position was approximately that shown in Figure 8(a).

[1] The DaVis software gives each experiment a file name based on the date and the time of day when it was acquired. The experiments in this report are referred to by the time (hh:mm:ss) only. The date of each experiment is given in Appendix 1.

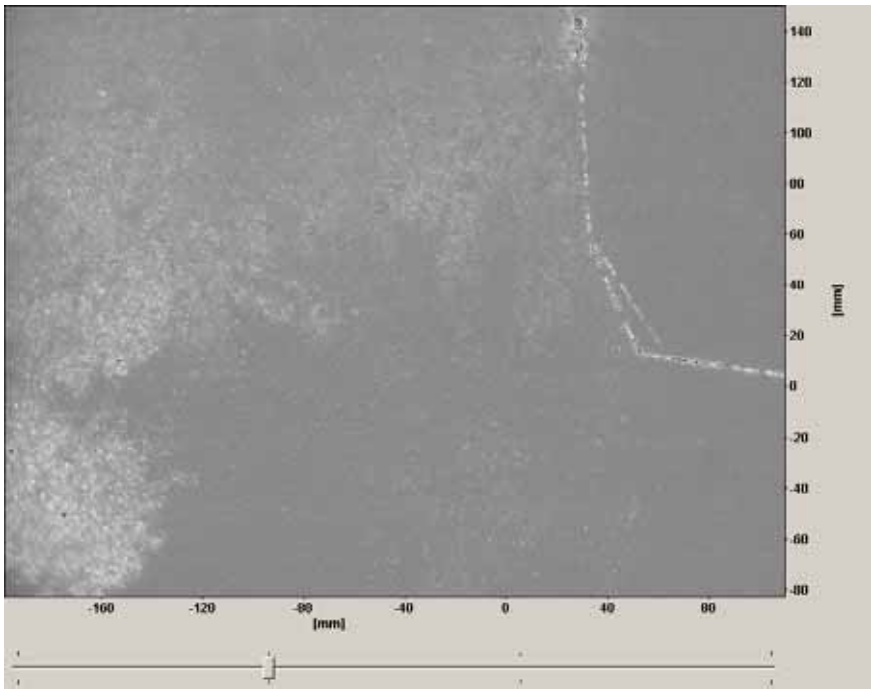

Figure 9(a), Run 15:29:35 Camera 1

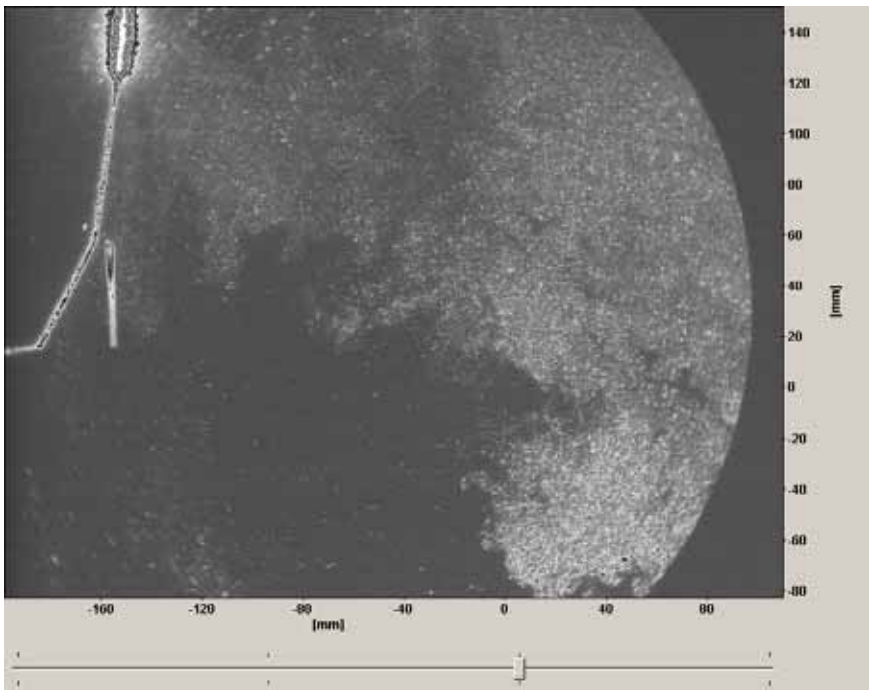

Figure 9(b), Run 15:29:35 Camera 2

4.0 SINGLE PIV MEASUREMENT WINDOW

4.1 Analysis Of Experiments

The analysis methods used in the *DaVis* software were described in detail (Molyneux (2006)). Data collection and preliminary analysis of the PIV experiments were carried out using the *DaVis* software package (LaVision, 2005). Complete processing of each data set before moving on to the next experiment was too time consuming. Individual frames were analyzed immediately after the experiment had finished, and selected runs were fully processed when a suitable gap between the experiments occurred, such as lunch breaks, or in the evenings. This preliminary analysis was enough to ensure that the data being collected was sufficiently accurate to be analyzed in more detail on completion of the experiment program.

The final data processing was in batch mode using the procedures described below. These settings were found to give consistent results for all the flow conditions tested. The final values of the settings within the software were determined using the combination of recommendations from LaVision and trial and error during the preliminary analysis.

Pre-processing of each image was carried out prior to calculating the velocity vectors. This consisted of subtracting a sliding background scale, based on 16 neighbouring pixels. When the vectors were calculated, the allowable range in pixels was zero plus or minus 10 for the x and y velocity components (within the measurement plane) and zero plus or minus 20 in the z velocity component (through the measurement plane). Vectors outside this range were excluded. Vectors were also excluded if the three-dimensional validation error was greater than 5 pixels. Vector post processing was based on an adaptive multi-pass method, with an initial window size of 64x64 pixels and a final window size of 32x32 pixels. Vectors were smoothed using a median filter with removal and replacement criteria based on two times and three times the RMS values of the eight neighbouring windows respectively. A second pass was made, based on the same allowable vector ranges, after the removal and replacement criteria had been applied once. This analysis gave consistent results through the experiment program, for the range of times between laser sheets used for the flow conditions studied.

Further vector processing was carried out to calculate the mean flow pattern across the complete time history of the measurements for each set of calculated vectors. This was carried out using the vector statistics function within *Davis* 7.1. This function required the specification of a minimum number of frames for which a vector must appear in order to include the value. After some preliminary investigations, the number used for this was 25% of the total number of frames taken. Based on trial and error, this level provided an acceptable compromise between data density over the full frame and the standard deviation of the vectors based on small samples. For the majority of the data runs, this value was 25 frames out of a total of 100, but for some of the early runs, this was 12 out of 50. The calculated vectors were exported from the *DaVis* PIV data collection and analysis software as *Tecplot* data files. *Tecplot* was used by for presenting of the results.

4.2 Discussion of Results

The most reliable interpretation of the experiment data should be on the basis of results at a single measurement window, since these required the minimum amount of data processing. Six key locations were identified from the results, where a single measurement window gave vectors that were important to understanding the flow around an escort tug hull with a large yaw angle.

All of the locations chosen for discussion were close to the hull. The results are presented on a grid relative to the complete measurement plane, rather than the grid for a single PIV window, so that the flow patterns can be more easily related to the position of the model and more easily compared from location to location. All the figures show vectors of in-plane velocity (V_x and V_y) and all the cases but one show repeat experiments superimposed on the same grid.

The discussion below is based on a single flow speed of 0.5 m/s, but as can be seen from the combined data sets that will be discussed later, the difference in flow pattern with speed was very small, although the magnitude of the flow velocity vectors changed.

a) Tug Without Fin, Upstream Side, Close to Waterline

Flow vectors for the upstream side of the tug (with no fin) between the waterline and the bottom of the hull are presented in Figure 10. Two sets of in-plane vectors at the same location are presented, and it can be seen that the mean flow vectors were coincident over almost all of the measurement space. This indicated that the mean flow measured in two separate data collection runs was stable over the complete measurement space.

Figure 10 shows that the flow vectors were generally directed away from the hull surface and downwards (in negative *x* and *y* directions) with little change in velocity magnitude. A region with rapidly changing flow direction is where the flow is starting to separate from the hull in the bottom right hand corner of the measurement window.

At this window location, it was found to be very difficult to get seed particles into the region just below the waterline and very close to the hull. The *z*-velocity in this region is low. Seeding particles introduced to the flow sufficiently far upstream of the measurement window to avoid unsteady flow caused by the rake did not reach the measurement window. This accounts for the absence of vectors in that region.

The three-fingered vertical rake was used for this location.

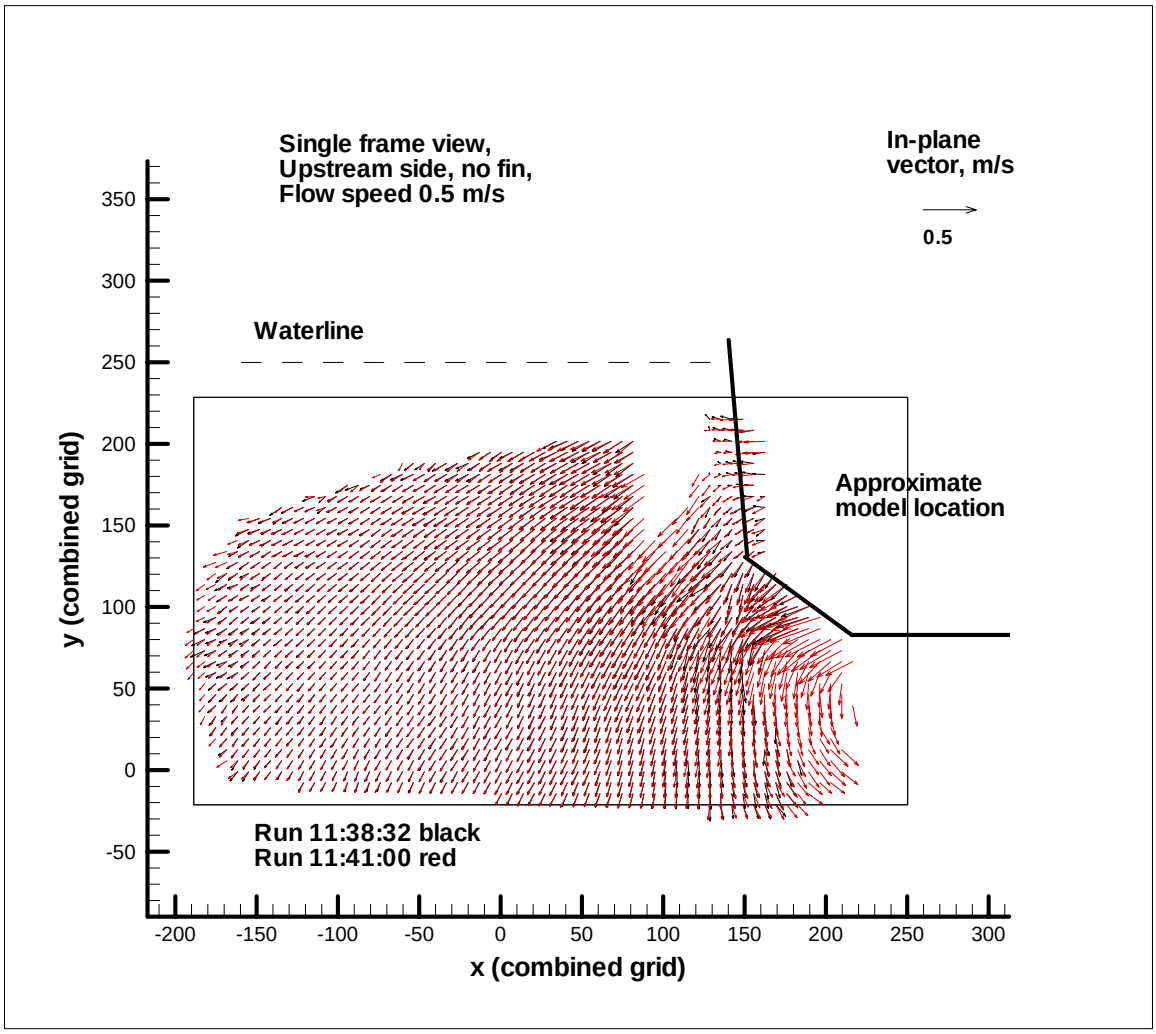

Figure 10, In-plane flow vectors, upstream side of hull without fin, bilge to waterline, flow speed 0.5 m/s

b) Tug Without Fin, Upstream Side, Under Hull

Figure 11 shows another region of the flow for the same conditions as Figure 10. The area of flow shown in Figure 11 is under the hull on the upstream side. This figure shows four distinct flow vectors in different parts of the measurement window. The first region is at the far left hand side where the flow is vertically downwards. The second region consists of a narrow band of fluid (approximately 50 mm thick) close to the hull, where the fluid was flowing towards the upstream bilge corner. The third region is immediately below the band of upstream flow. In this region the flow is rapidly changing speed and direction. Over the rest of the flow measurement window the flow direction is from top left to bottom right.

This figure reinforces the observation made in Figure 10 that the flow is separating off the upstream bilge corner. Figure 11 shows areas of rapidly changing flow speed and direction and it is likely that a vortex was formed under the hull, although the circulation pattern is incomplete, and likely extends beyond this measurement window.

Figure 11 shows two sets of measurements superimposed, and as in Figure 10 there is very good overlap of the calculated flow vectors. To obtain this PIV result, the three-fingered horizontal seeding rake was positioned under the model.

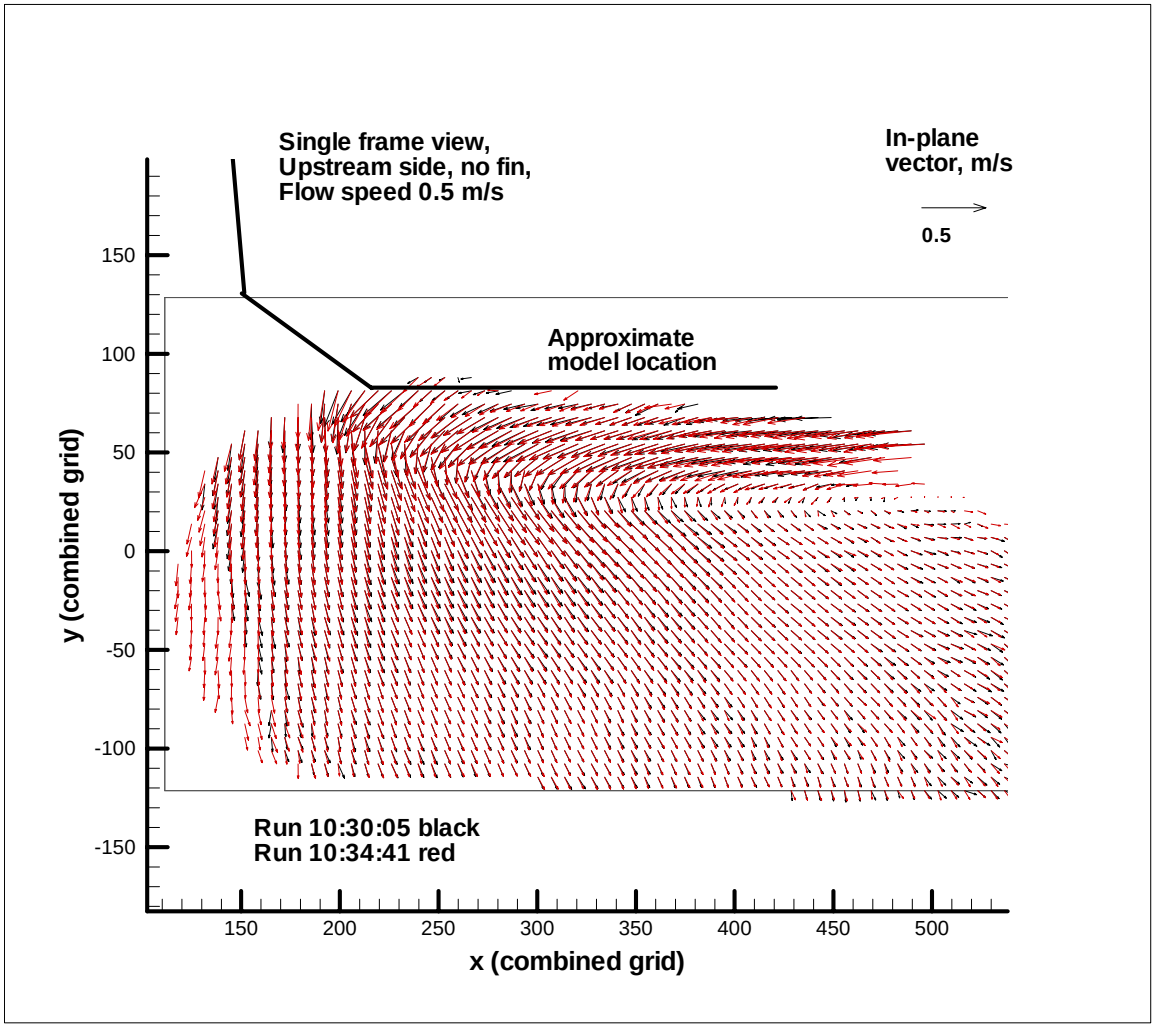

Figure 11, In-plane flow vectors, upstream side of hull without fin, under hull, flow speed 0.5 m/s

c) Tug Without Fin, Downstream Side, Close to waterline

Figure 12 shows the flow vectors on the downstream side of the hull, with no fin, from the bilge to the waterline. This figure shows the development of a vortex close to the downstream side of the hull, caused by the flow separating off the corner of the bilge. The rest of the figure shows a strong upward flow component in the lower right hand corner and a horizontal flow component entering the window from the far left hand side.

Seeding in this situation proved to be extremely challenging when only one rake was used. For the view given in Figure 12, the 3-fingered vertical seeding rake was situated close to the waterline. This arrangement resulted in the absence of vectors in the lower right hand corner, which would have completed the definition of the flow around the core of the vortex.

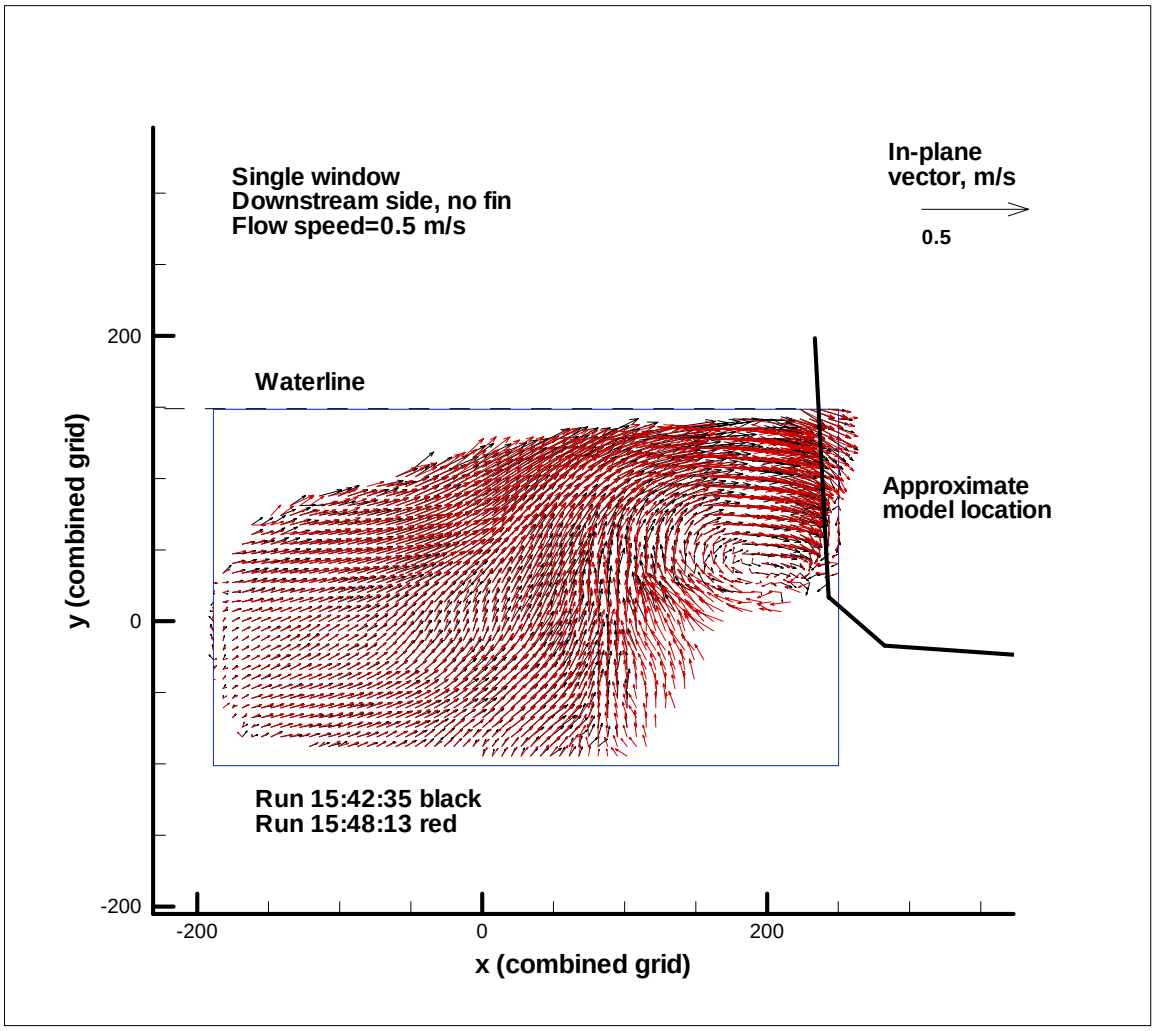

Figure 12, In-plane flow vectors, downstream side of hull without fin, bilge to waterline, flow speed 0.5 m/s

d) Tug Without Fin, Downstream Side, Under Hull

The flow patters for the region under the downstream bilge corner are shown in Figure 13. This region is under the one shown in Figure 12. Figure 13 shows that the flow has a strong upward component over almost the entire measurement window. The only area where the flow changes direction is on the downstream corner of the bilge, where the upward flow vectors are redirected into an almost horizontal direction when the flow encounters the hull. It is likely that this strong horizontal flow, off the downstream bilge corner is the major contribution to the formation of the vortex shown in Figure 12. Other than this redirection of the flow in the top right-hand corner of the window, the flow is almost uniformly upwards.

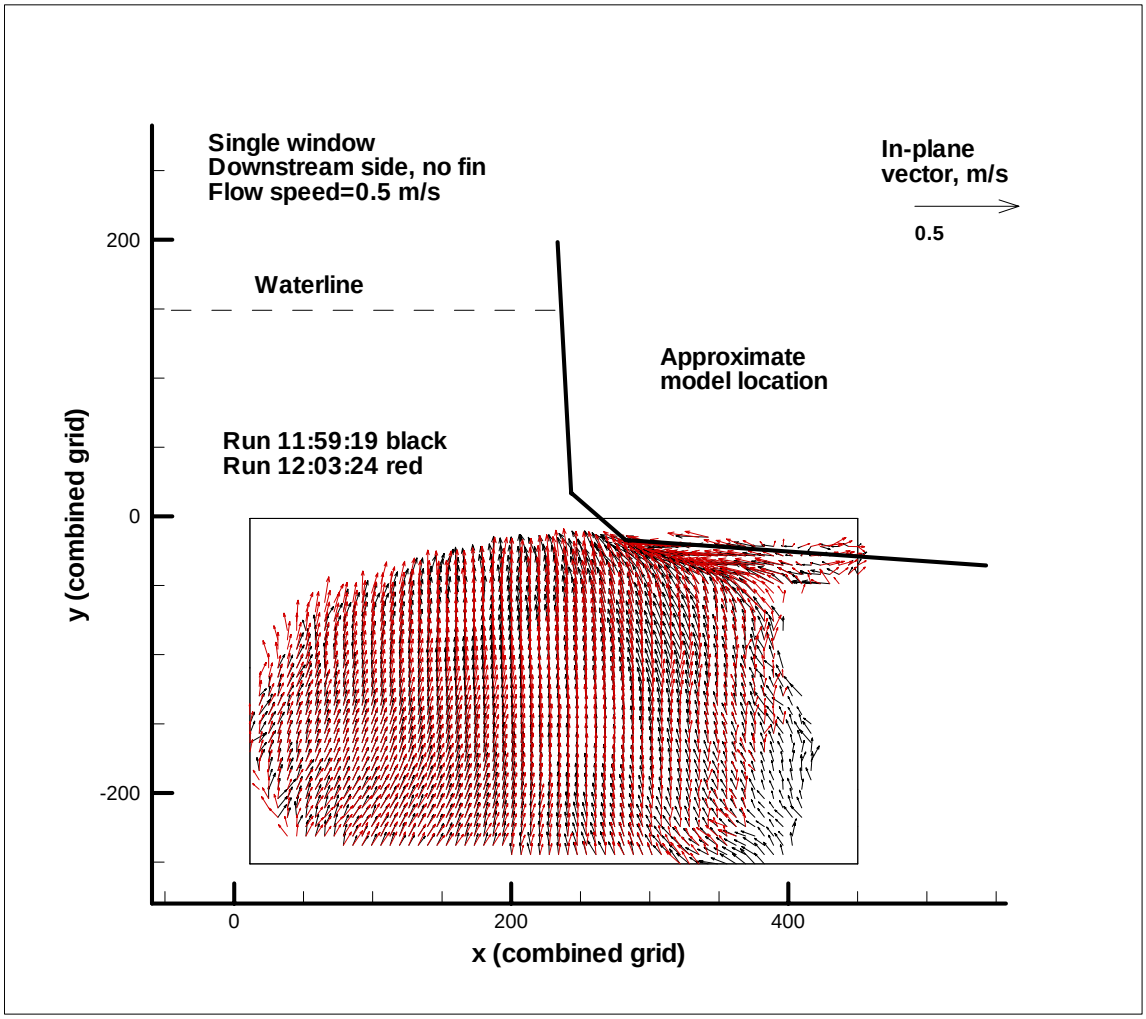

Figure 13, In-plane flow vectors, downstream side of hull without fin, under hull, flow speed 0.5 m/s

For the view in Figure 13, the horizontal seeding rake was used located well under the model. The view given in Figure 13 shows that the flow entering the region, which was undefined in Figure 12 is coming from a completely different direction than the rest of the flow in Figure 12. The full definition of vectors within the window given in Figure 12 would have required two seeding rakes to be operated simultaneously.

e) Tug With Fin, Downstream Side, Close to Waterline

The flow patterns on the downstream side of the hull with the fin fitted, between the waterline and the bilge corner, are shown in Figure 14. The flow is relatively uniform with an upstream component (from left to right) back towards the hull, with some curvature, so that the flow is upwards on the left hand side, but horizontal on the right hand side.

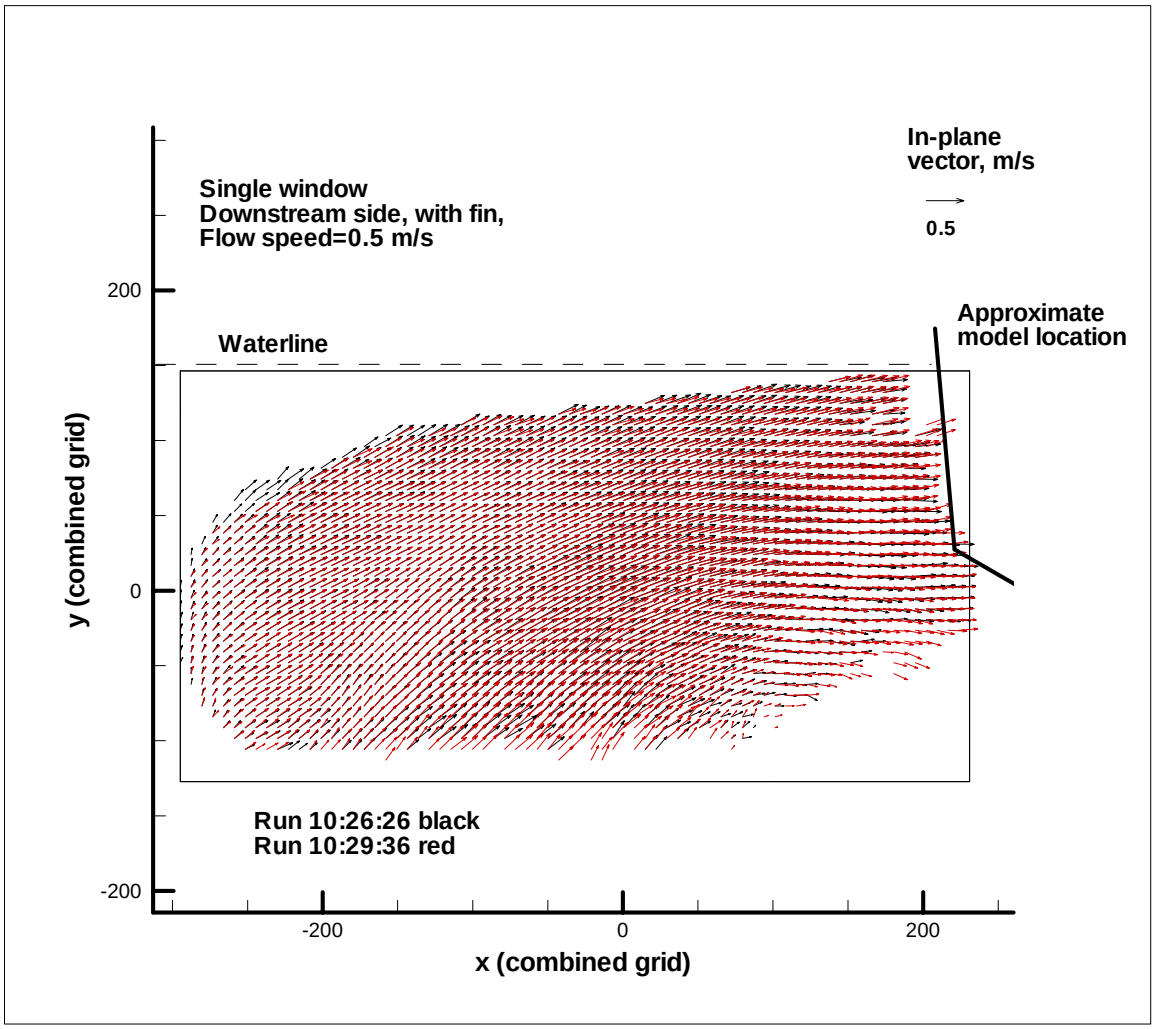

Figure 14, In-plane flow vectors, downstream side of hull with fin, bilge to waterline, flow speed 0.5 m/s

Comparing Figures 12 and 14 shows the effect of the fin on the flow in this region, between the waterline and the downstream bilge. Figure 14 shows no sign of the vortex caused by flow separating off the bilge corner that was seen in Figure 12.

f) Tug With Fin, Downstream side, Under Hull

The flow patterns under the hull, on the downstream side, are shown in Figure 15. This figure shows the presence of a large vortex, centred under the edge of the hull. This vortex was contained within a single measurement window, and the two different data sets give the core at approximately the same location. Comparing Figure 15 with Figure 13 shows one effect of fitting the fin, as this large vortex was not seen in Figure 13.

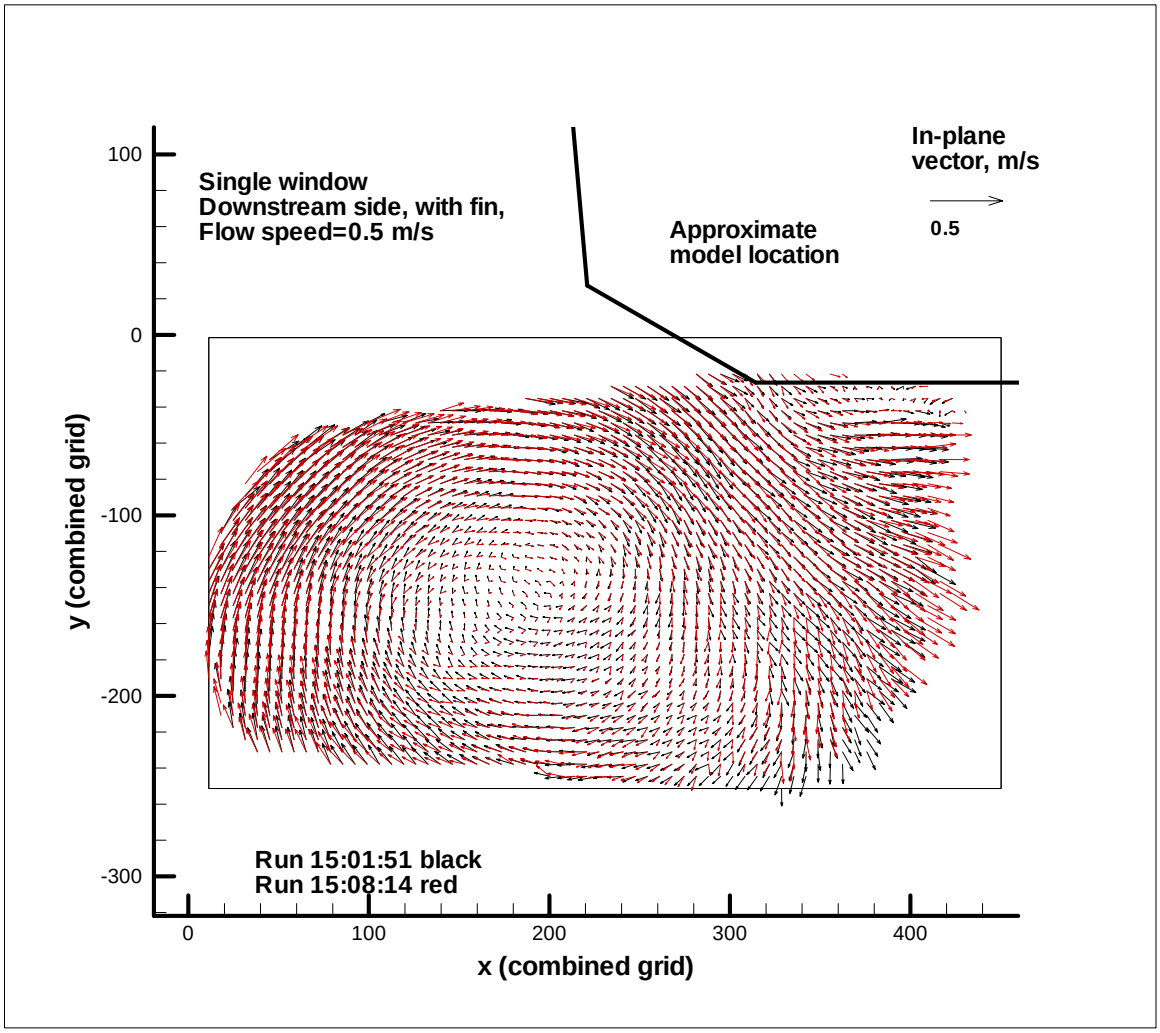

Figure 15, In-plane flow vectors, downstream side of hull with fin, under hull, flow speed 0.5 m/s

A second view of the flow in this condition is shown in Figure 16. The location for this view was even further under the hull than the view given in Figure 15. Only one experiment was available for this location but it is included in the discussion because it shows some complex flow patterns. The upstream flow component at the top of the vortex can be seen to separate off the downstream bilge corner, so the flow away from the hull is moving upstream, but the flow close to the hull is moving downstream. This is the opposite direction to the vortex observed on the upstream side of the bilge, so this indicates the presence of two regions of separated flow on the underside of the hull caused by the bilge corners when the fin is fitted.

Seeding rake location for these views was approximately the same as for the case when the fin was removed.

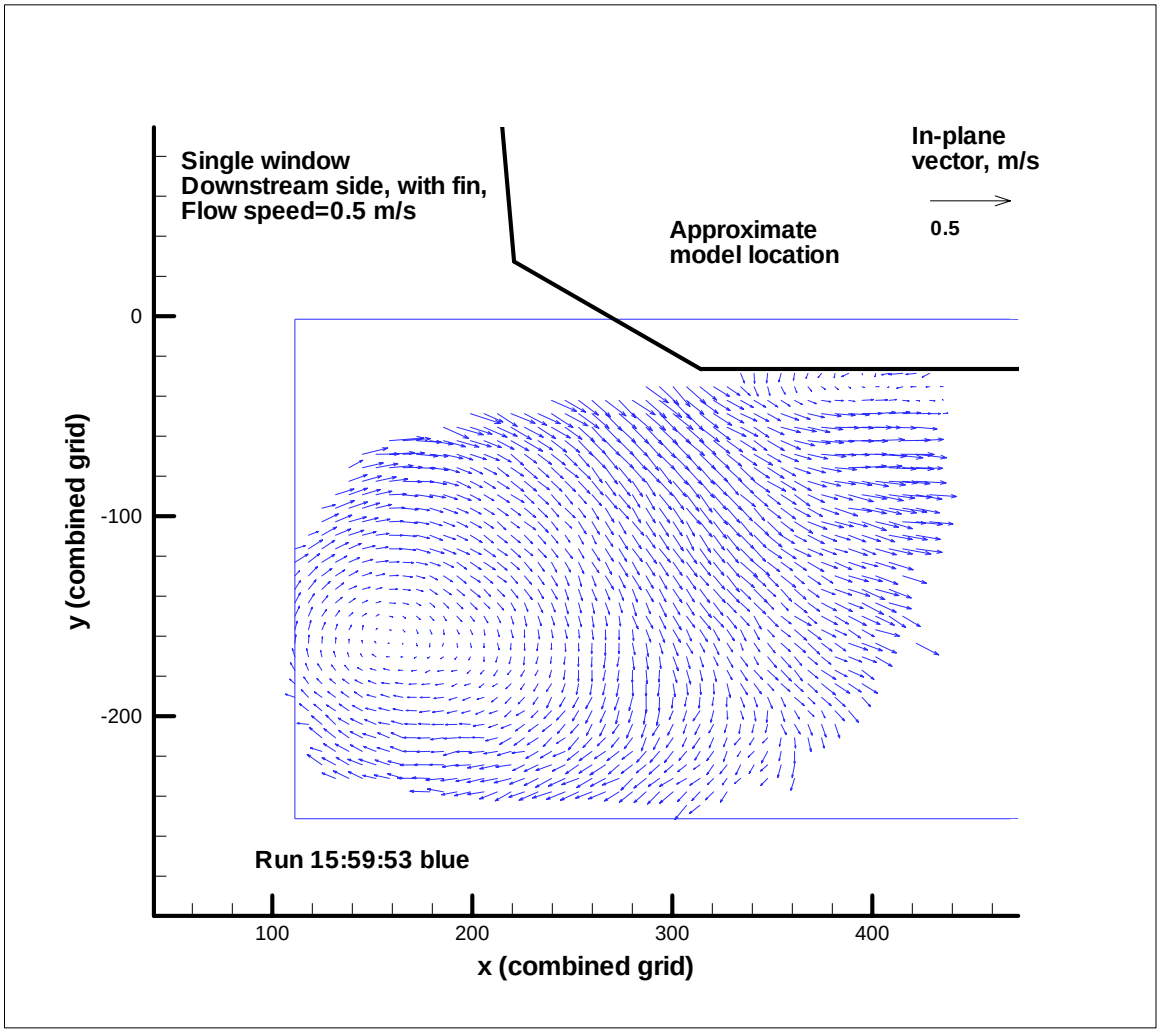

Figure 16, In-plane flow vectors, downstream side of hull, with fin, under hull, flow speed 0.5 m/s

This location, under the hull on the downstream side, with the fin fitted, showed the greatest discrepancy between the two vector sets for different data sets. Figure 15 shows more difference between the two sets of vectors than any of the other cases presented, as can be seen when Figure 15 is compared to the other figures. The extent of the unsteadiness in the flow at this location will be discussed below. The more turbulent flow actually aided seeding, since it tended to mix the seed particles, and resulted in a relatively even particle distribution over the measurement window.

5.0 OVERLAPPED PIV WINDOWS

5.1 Data Analysis

The complete flow pattern for the area of interest around the escort tug model was larger than a single window of the PIV system. Extending the measurement area beyond a single window required several movements of the model relative to the PIV system, and two depths of submergence for the PIV system within each plane. When the increments of model movement in each direction were approximately one third of the dimension of the window (100mm). As a result a small area of the flow, relative to the model, should occur in at least three separate measurement windows.

The first step in the process of combining all the data within a measurement plane was to add the shift of the model (relative to the PIV measurement space) to the x and y coordinates obtained from the PIV window. The specific movement of each PIV system window to convert all the data from one measurement plane into a common grid system is given in Appendix 1.

The flow patterns obtained from different measurement windows at the same coordinates in the measurement plane were then compared. This was done by plotting the overlapped windows and comparing the measured velocity components. An example of some overlapped windows, for flow measurements on the downstream side of the hull, with no fin, is given in Figure 17. The vectors given were the average values for each window, using the thresholds discussed above. In general, the agreement between flow measurements for overlapped windows was very good, even when the flow conditions were highly unsteady.

The *DaVis* analysis software gave zero values for points where there was insufficient seeding to define the flow. These points had to be removed before integrating the data from different windows, otherwise the interpolation routine would include erroneous zero values for an area in one window where the same area had a valid non-zero value in another window covering the same area, but where the seeding was present. To remove these zero values, the magnitude of the flow velocity at each grid point was calculated, and points with zero flow magnitude were removed.

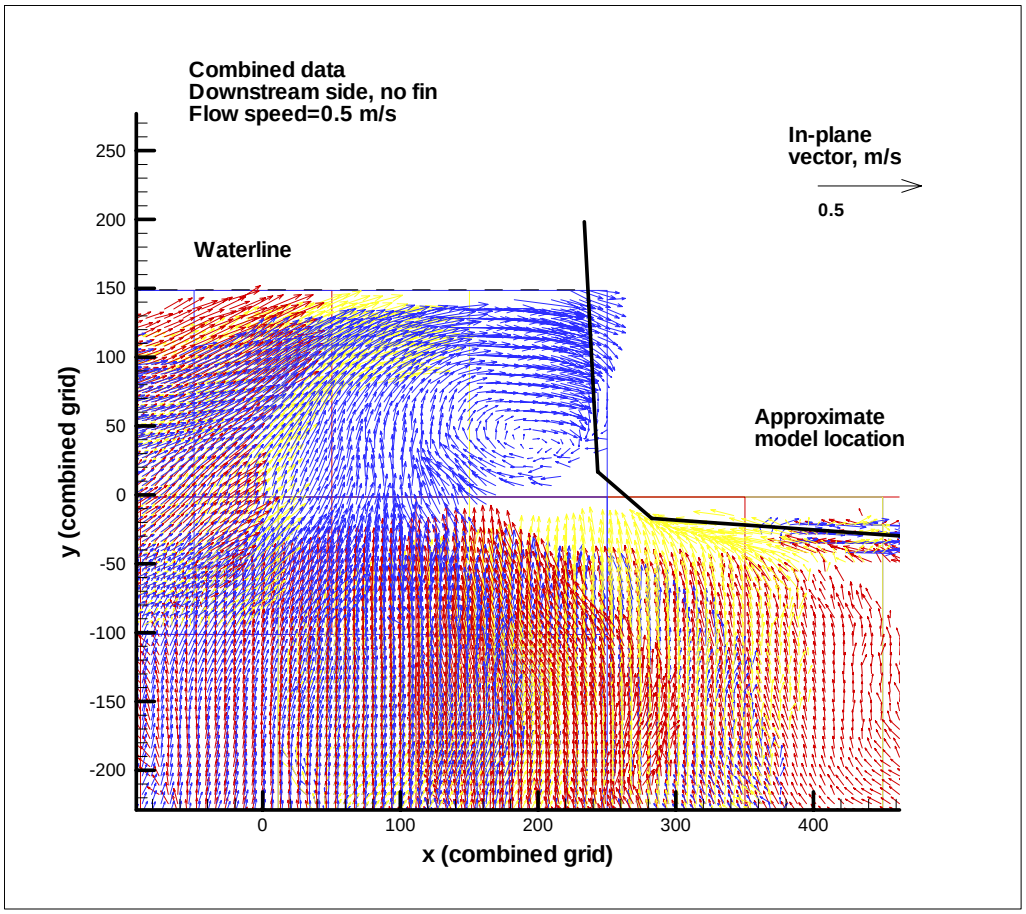

Figure 17, Example of overlapped windows, mean vectors for in-plane flow

The reduced data sets (excluding the zero flow magnitude cases) were combined and plotted as contours of velocity component (V_x, V_y, V_z). Examples of contour plots of the combined data for flow measurements on the downstream side of the hull with no fin, at a flow speed of 0.5 m/s are given in Figures 18a) to 18c).

The contour values were interpolated on a larger scale grid, which extended over the full measurement space. The interpolated velocity components were re-combined into three-dimensional vectors and compared with the original data to check for any significant errors or discrepancies. An example of the comparison between the interpolated vectors for the in-plane flow and the vectors obtained from the PIV system is shown in Figure 19. The example given is for the same flow conditions shown in Figures 18a) to c). The data interpolation was carried out using *IGOR* (Wavemetrics, 2004) and the display of the final combined data set on the revised grid was made with *Tecplot*.

The grid size can be chosen depending on the nature of the flow being studied. For all the cases given here, the grid spacing presented was on 20mm squares. This grid can be the basis for detailed comparisons of the vectors calculated from the PIV experiments with CFD predictions for the flow.

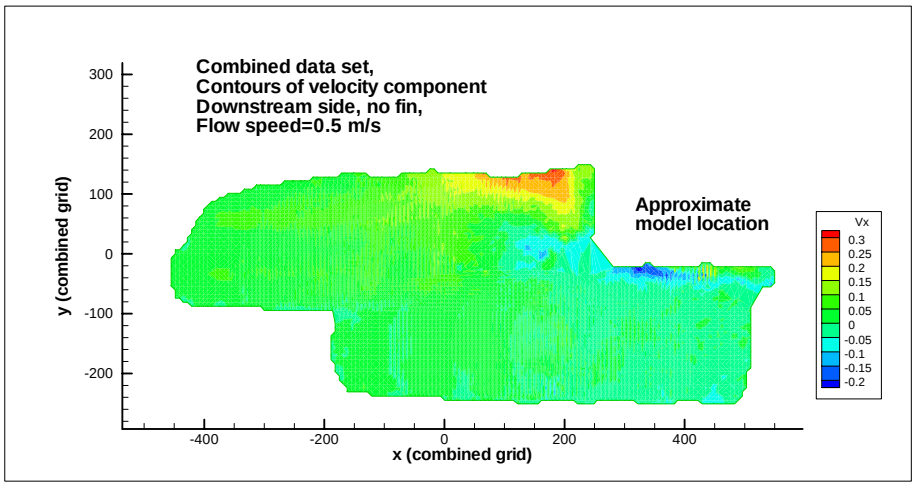

a) x-velocity component

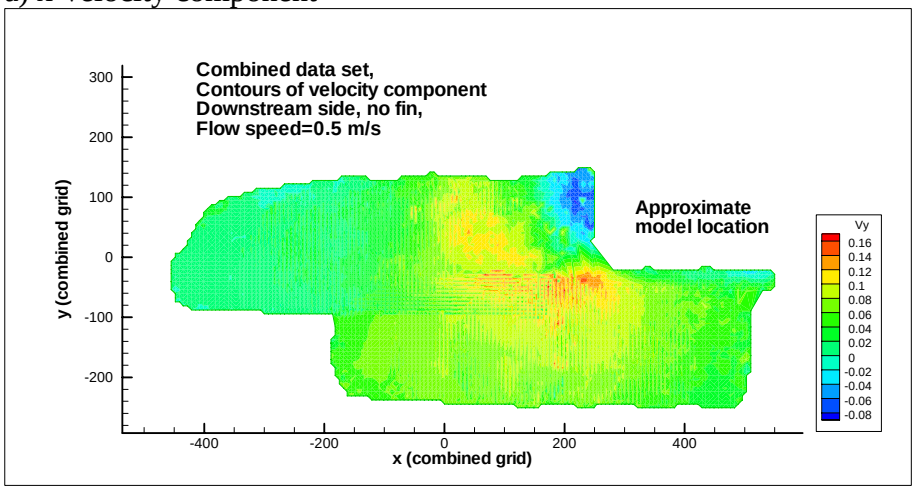

b) y-velocity component

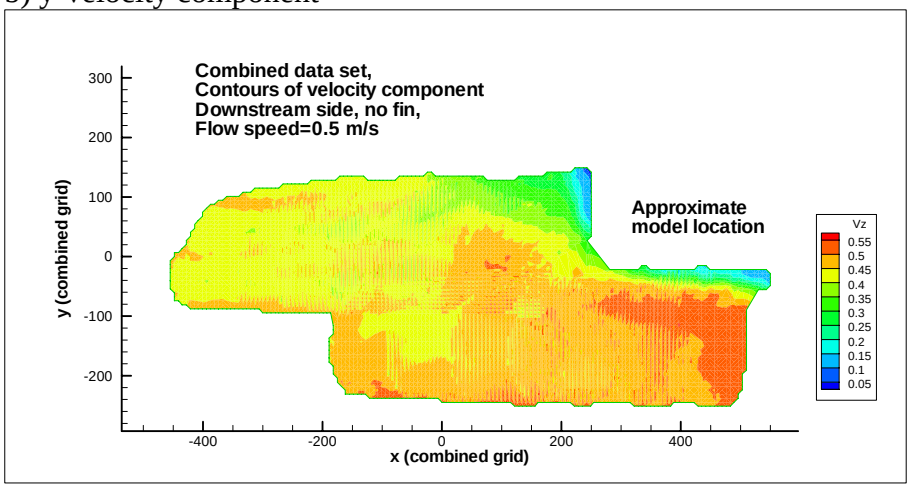

c) z-velocity component

Figure 18, Contours of velocity component, from overlapped windows

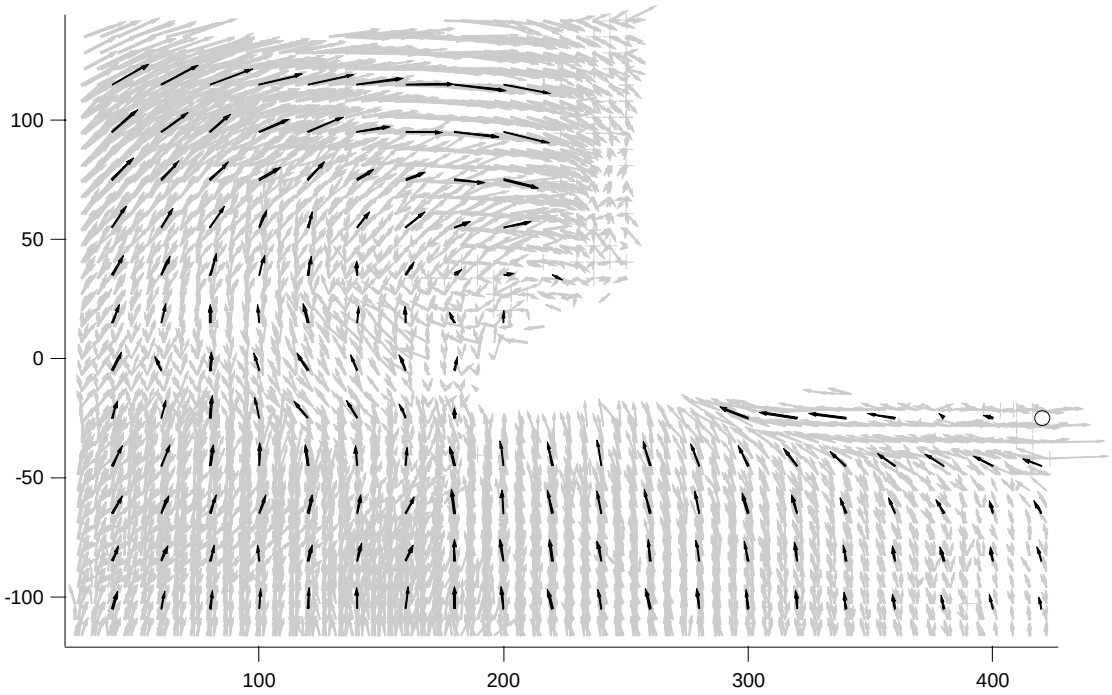

Figure 19, Comparison of in-plane vectors from combined experiment data (grey) with interpolated vectors (black), downstream side without fin, flow speed=0.5 m/s

5.2 Discussion of Results

a) Upstream Side Without Fin

The combined results for the upstream side of the hull, without the fin fitted are shown in Figures 20 and 21. Figure 20 includes the results for the cases shown in Figures 10 and 11. The combined results show the in-plane flow features, such as the flow away from the hull surface in the region of the flow close to the hull and the waterline, the separation of the flow from the upstream bilge corner and the upstream flow component close to the underside of the hull that have already been discussed. Also shown in Figures 20 and 21 are contours of through plane velocity. The through plane velocity is very low, close to the hull surface, but accelerates as it passes the underside of the hull.

b) Downstream Side Without Fin

The combined results for the downstream side of the tug, without the fin, are shown in Figures 22 and 23 for vectors of in plane flow components and contours of through plane flow speed. There are two dominant flow directions in these figures. One is an upward vertical flow under the hull, and downstream from the hull in the lower region of the measurement space. The other is a horizontal upstream flow, which was strongest close to the model and the water surface, which decreases further downstream. Figures 22 and 23 also show the presence of a vortex on the downstream side of the hull, caused by the flow separating off the downstream bilge corner. This vortex extends from the underside of the hull to the waterline.

Figure 22 includes the results shown in Figures 12 and 13.

c) Downstream Side With Fin

The combined results for the downstream side, with the fin fitted are shown in Figures 24 and 25. Both figures show the presence of a well-defined vortex located under the downstream bilge corner, which extends the full depth of the combined measurement window. Figures 24 and 25 also that the upstream in-plane velocities close to the water surface are stronger than for the case for the hull without the fin. When the fin is fitted, the effects of the hull on the flow are seen further downstream from the hull than when the fin is removed.

Overall there is little change in the flow patterns with speed for the two speeds tested, but the magnitudes of the vector components change with the undisturbed flow speed. The biggest difference was for the case shown in Figures 24 and 25 for the downstream side of the hull with the fin fitted. Here, the region of low speed flow extended further away from the downstream side of the hull at 1 m/s than at 0.5 m/s.

Figure 24 includes the results shown in Figures 14, 15 and 16.

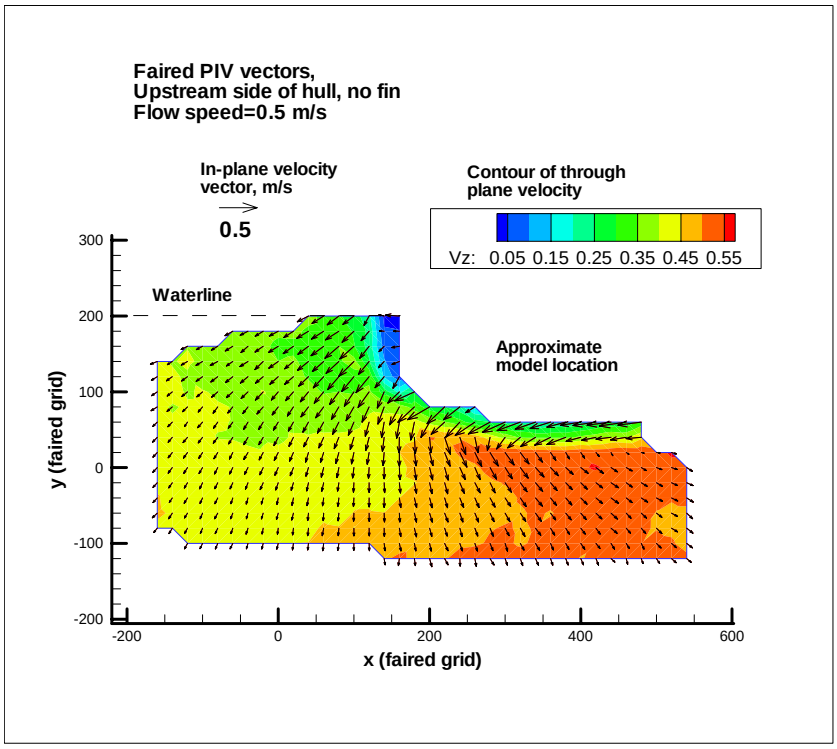

Figure 20, Faired vectors, upstream side, no fin, 0.5 m/s

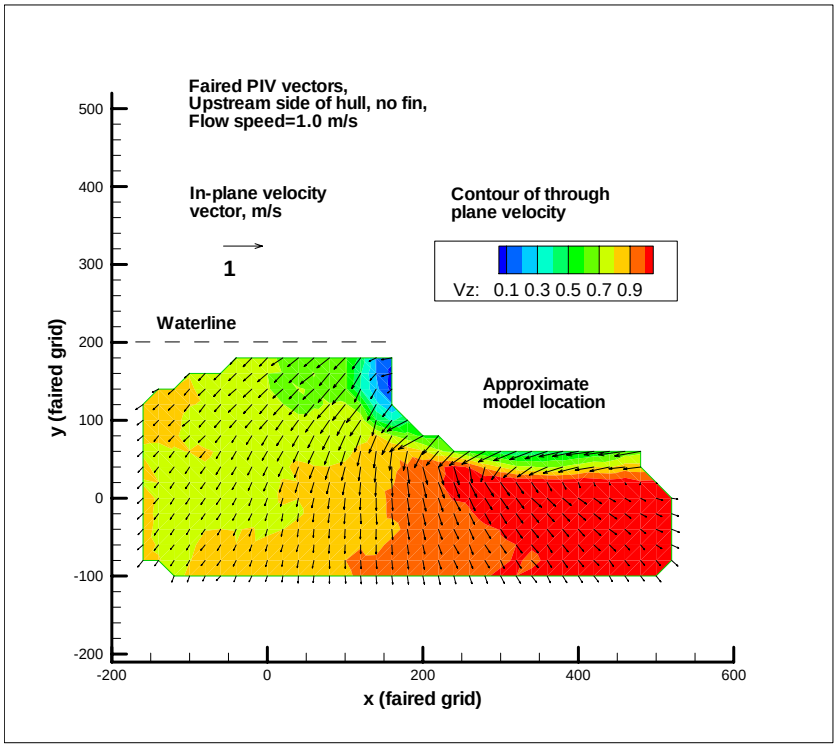

Figure 21, Faired vectors, upstream side, no fin, 1.0 m/s

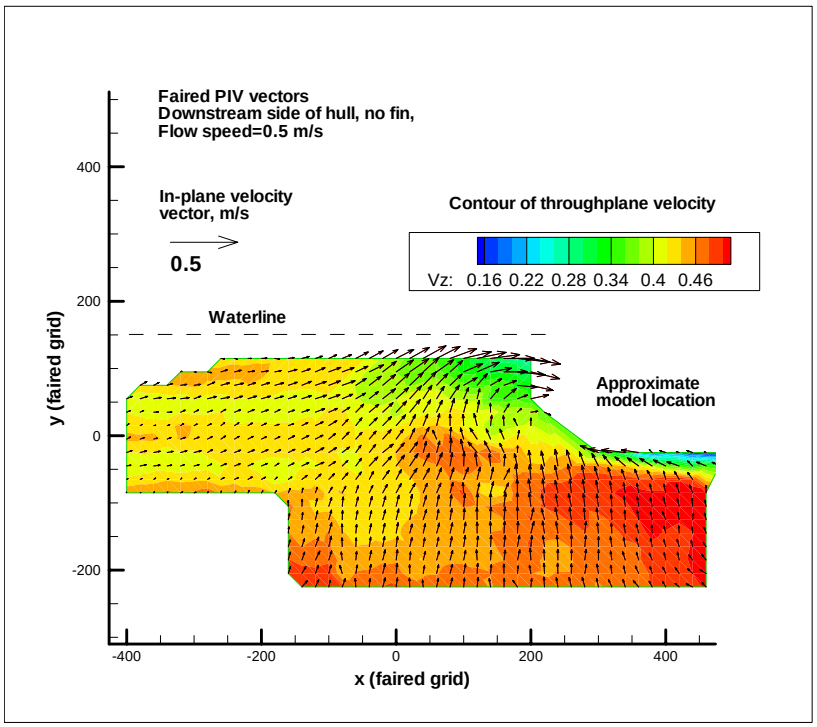

Figure 22, Faired vectors, downstream side, no fin, 0.5 m/s

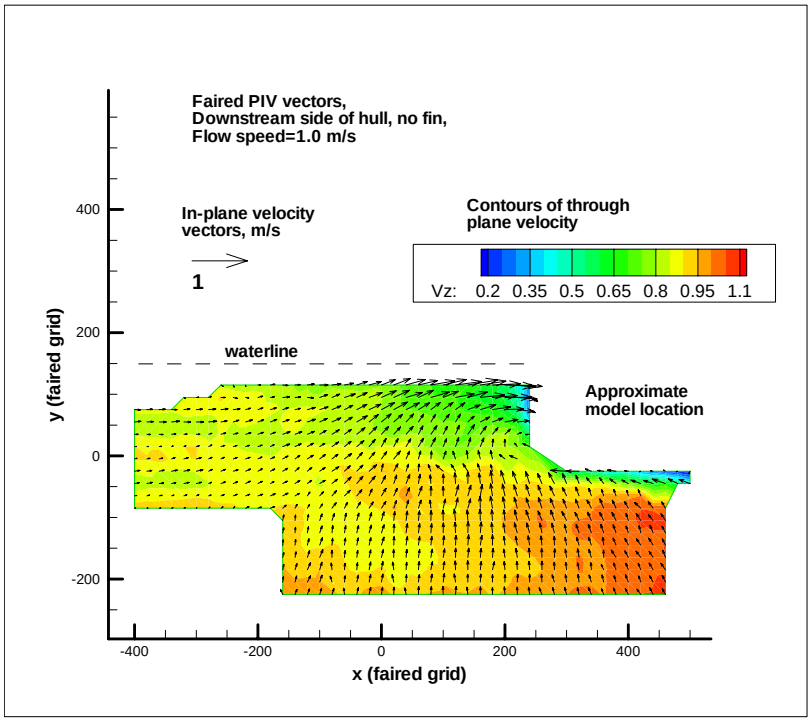

Figure 23, Faired vectors, downstream side, no fin, 0.5 m/s

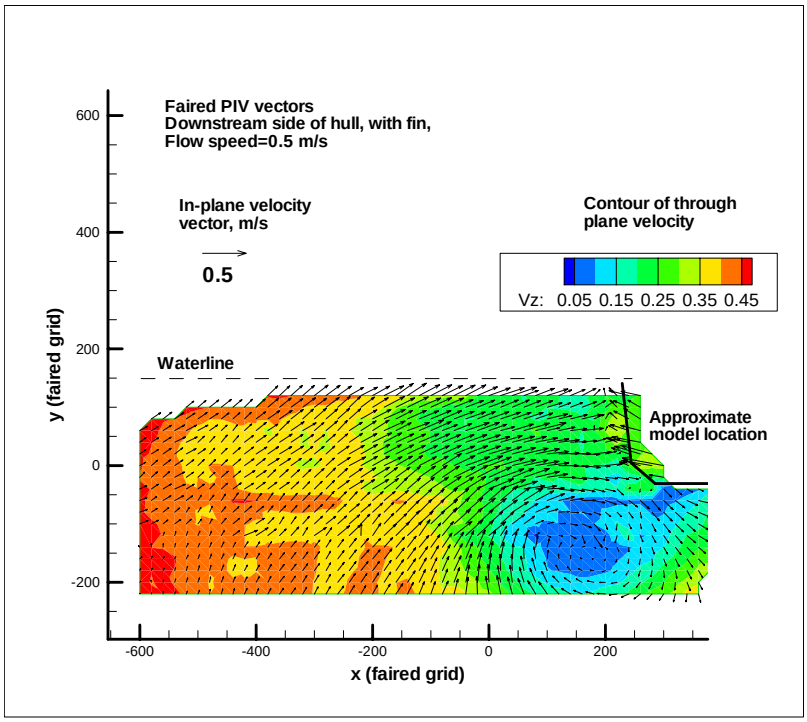

Figure 24, Faired vectors, downstream side, with fin, 0.5 m/s

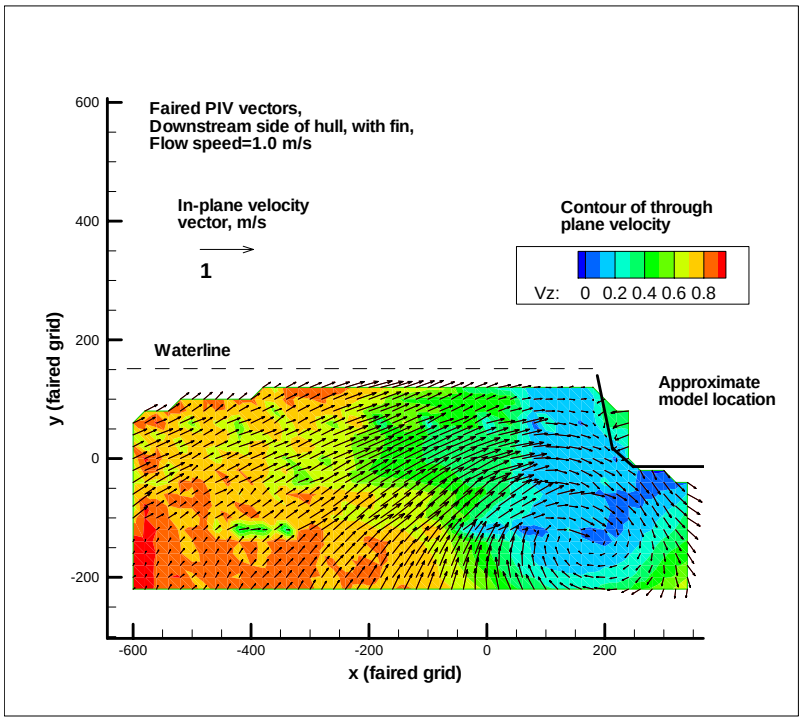

Figure 25, Faired vectors, downstream side, with fin, 1.0 m/s

d) Fairing of Multi-Windowed PIV Data

Overall, the fairing process retained the essential features of the flow based on the vectors derived from the single PIV windows discussed above. There was some smoothing of the flow patterns when compared to the single windows. An example of this is the flow on the downstream side of the hull with the fin removed (Figure 22), which can be compared to the raw data (Figure 12). The flow within the vortex shown in Figure 22 has been smoothed out because the faired flow was based on the average vectors from several overlapped windows.

The advantage of the faired data was that it was based on vectors averaged over several overlapped analysis windows. As a result small variations in the flow patterns caused by distortions of the PIV image close to the edge of an analysis window, or differences in flow patterns caused by different rake designs and locations will be averaged out.

The smoothing process does result in the occasional vector that does not match the size or direction of those around it. This was caused when overlapping windows gave conflicting vector information for the same location. This typically occurred in regions where the flow was sparsely defined and the vectors from different windows were in different directions. This could have been caused by two factors. One factor was that the flow was unsteady and different average vectors were obtained for the same region, as was the case in Figure 15, where although the vortex was well defined in each experiment, the centre of the vortex was not at the same location. The other factor was that the same region could be have been seeded with different seeding rakes, and in some cases, the change in seeding rake may have changed the resulting local flow vectors, if it was too close to the measurement region. These slight anomalies could be removed with further processing. This would require comparing each vector with its nearest neighbours and only allowing certain variations in the flow pattern in a manner similar to that used in the post-processing of the PIV data.

It is intended that the combined results discussed in this section will be compared with CFD predictions for the same flow conditions over the same spatial region. The loss of detail in some parts of the flow can be overcome by reducing the area of comparison to the area of a single window in the region of interest. The complete data set was required to check the consistency of the results over the full measurement space, which was much larger than the single measurement window.

6.0 UNSTEADY FLOW

The average vectors for run 15:01:51 are shown in Figure 26, for the case of the tug with the fin on the downstream side of the hull. The vortex shown in this figure was also shown in the results of run 15:08:14, which was obtained at exactly the same location. The two results are shown together in Figure 15. The individual time steps that went to make up this average pattern showed the degree of variation of the flow pattern with time. This is illustrated by a sample of twelve consecutive vector images taken from run 15:01:51 and shown in Figures 27(a) to 27(l). These figures show that a vortex is visible in some figures, for example Figures 27(d) to 27(h). In some of the other figures the vortex is not seen at all, for example Figures 27(i) to 27(l). These twelve images when combined with the rest of the data set show that the average pattern is the well-defined vortex shown in Figure 26. So even though the flow was unsteady, the long-term average was relatively stable, which is the classical definition of turbulent flow, and provides a justification for using RANS codes to analyze the flow conditions.

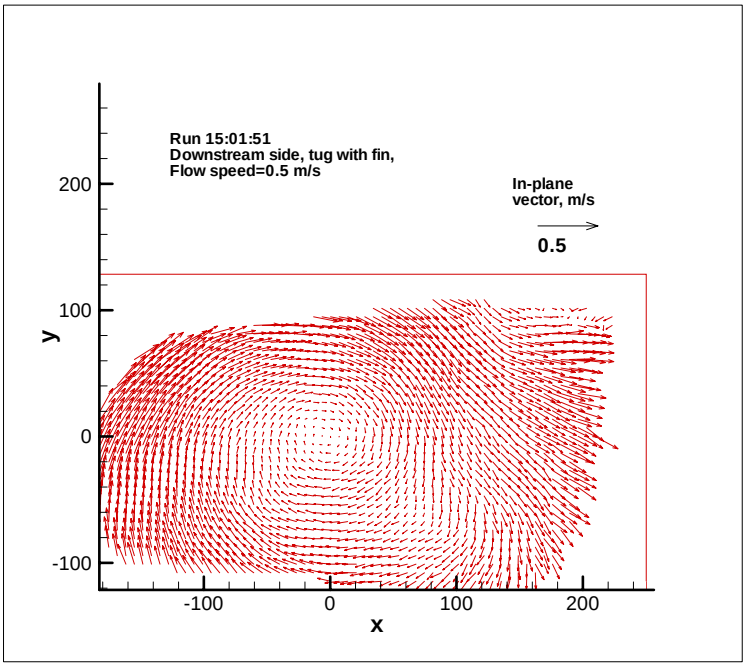

Figure 26, Run 15:01:51, Vector average over 100 frames, with 25 frame threshold

It was expected that the flow around the escort tug hull would be unsteady, based on visual observations made during earlier experiments (Molyneux, 2003, Molyneux and Xu, 2005) but a numerical quantification of the level of unsteadiness was unknown. It is generally accepted that PIV systems are unsuitable for providing a numerical definition of the turbulence (Van den Braembussche, 2001) because the sampling rates are too low to capture high frequency variations, but one measure of the unsteadiness in the flow that was obtained from the *DaVis* software (LaVision, 2005) is the RMS value of the vector components. Areas of flow with high RMS values will be areas of high turbulence although a true numerical estimate of the turbulence cannot be made.

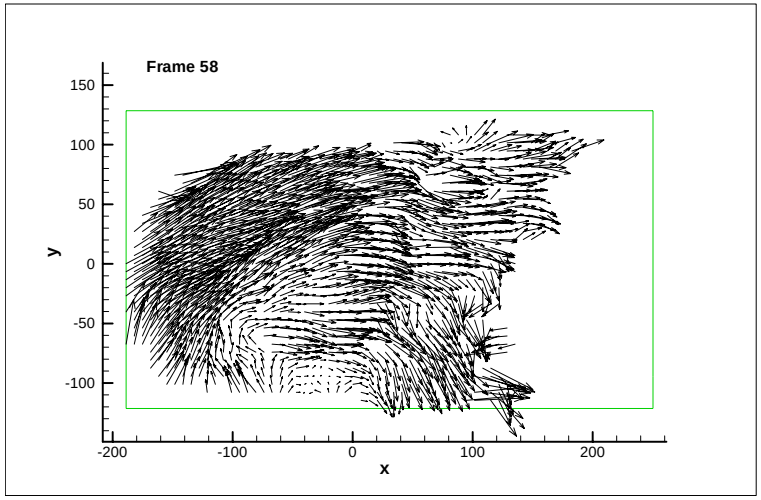

a)

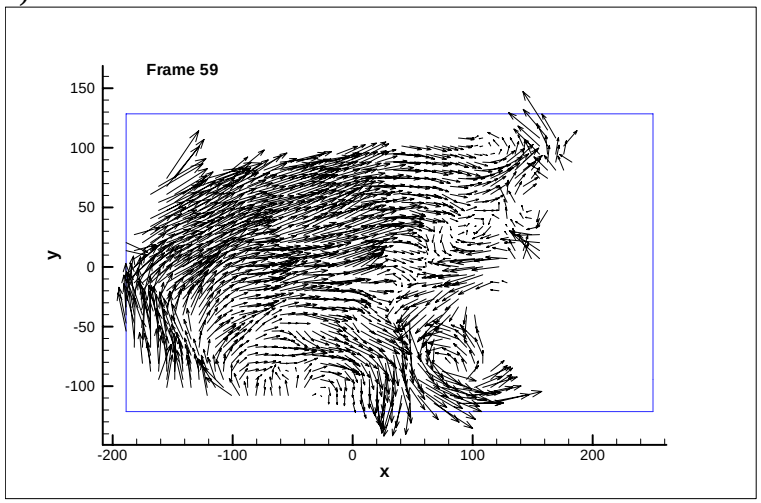

b)

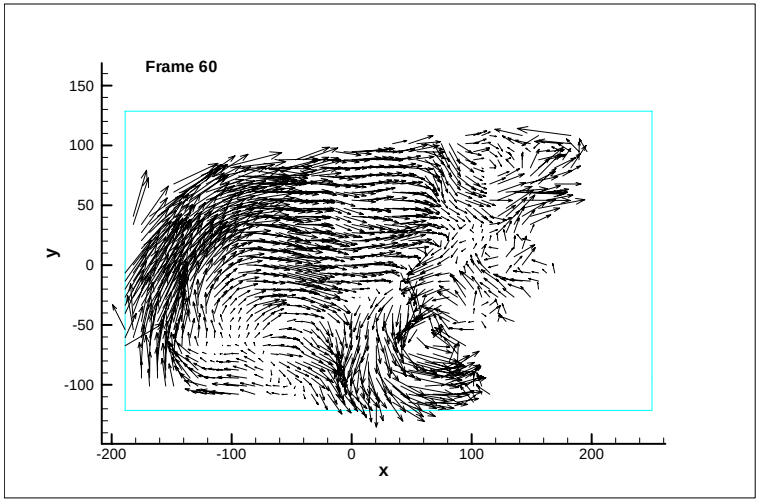

c)

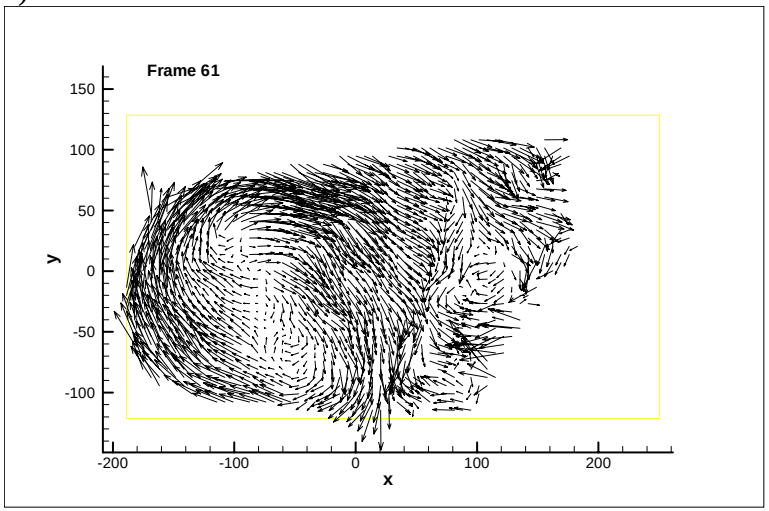

d)

Figure 27, Run 15:01:51, Consecutive time steps at 1000 μs intervals

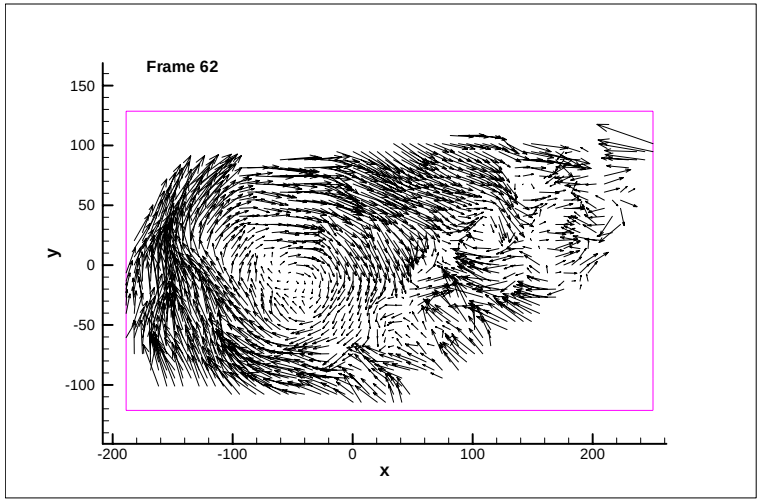

e)

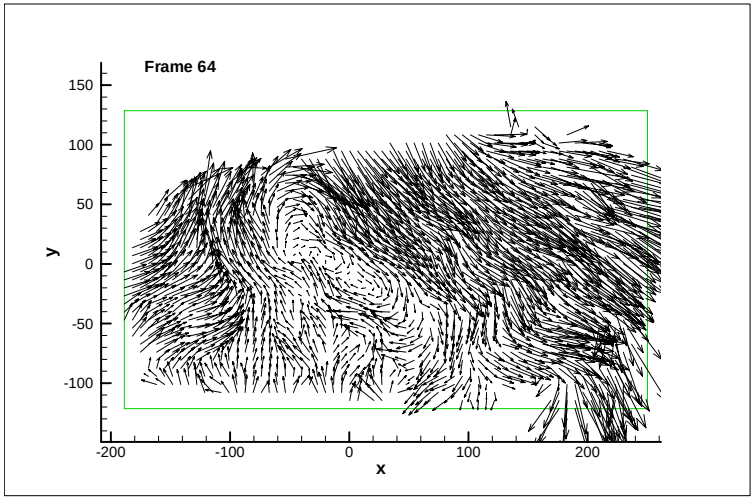

g)

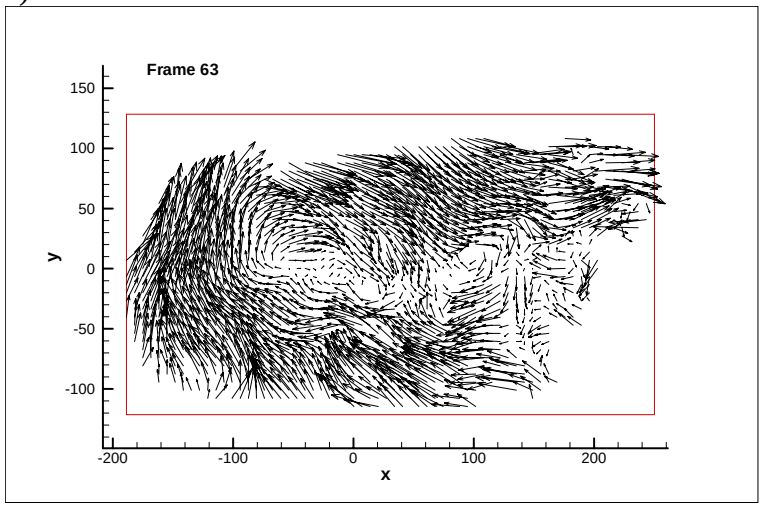

f)

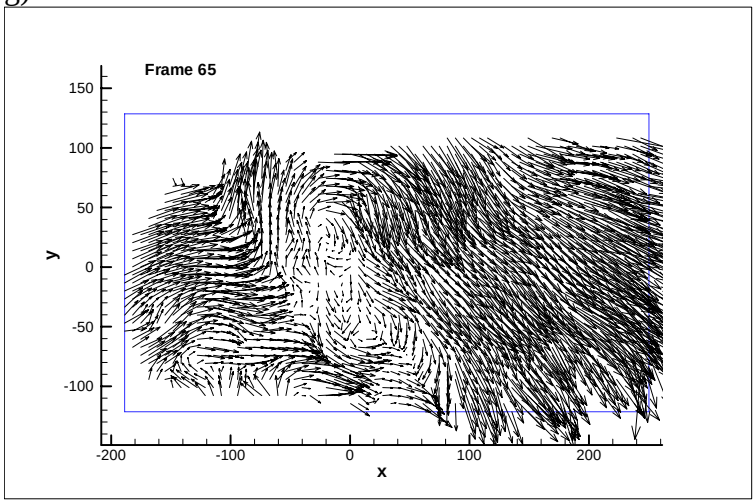

h)

Figure 27, Run 15:01:51, Consecutive time steps at 1000 μs intervals

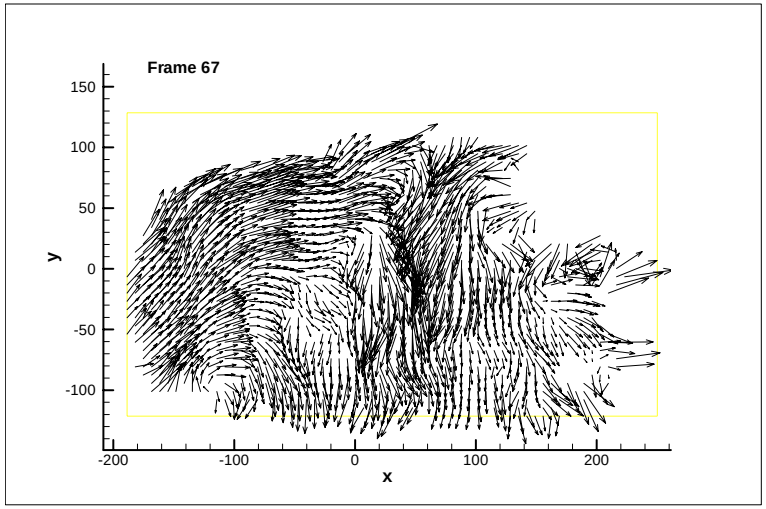

i)

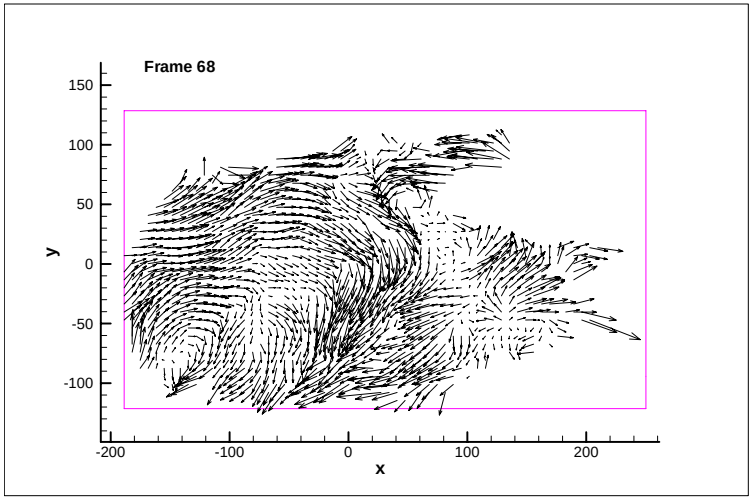

k)

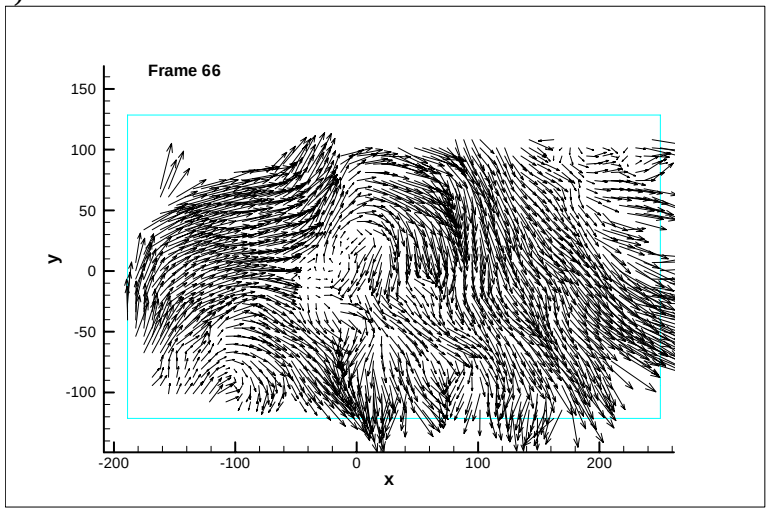

j)

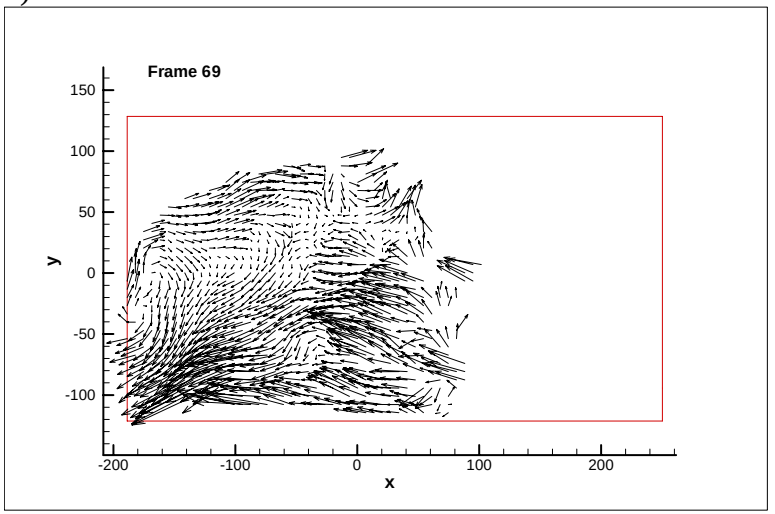

l)

Figure 27, Run 15:01:51, Consecutive time steps at 1000 μs intervals

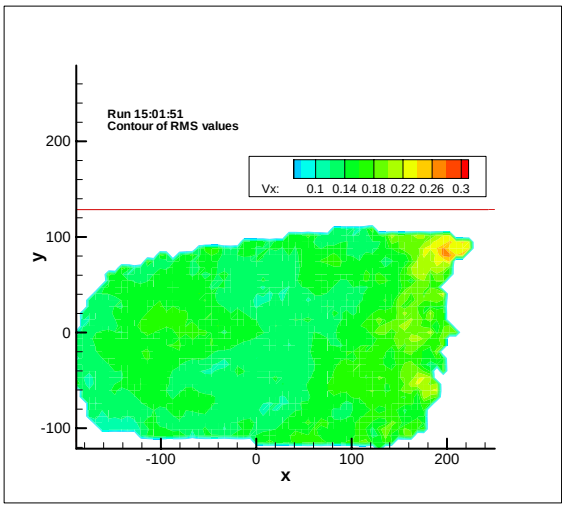

a) Vx

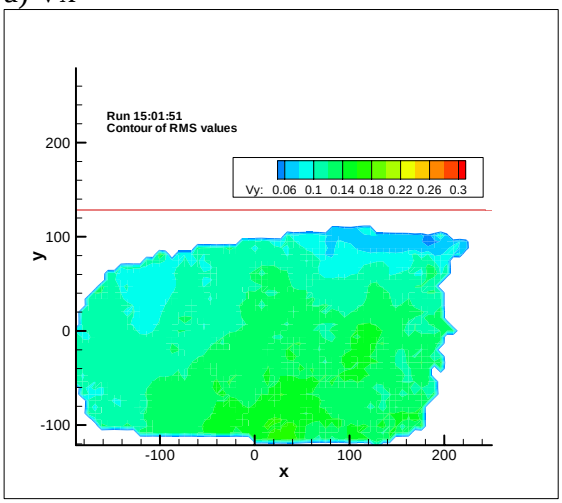

b) Vy

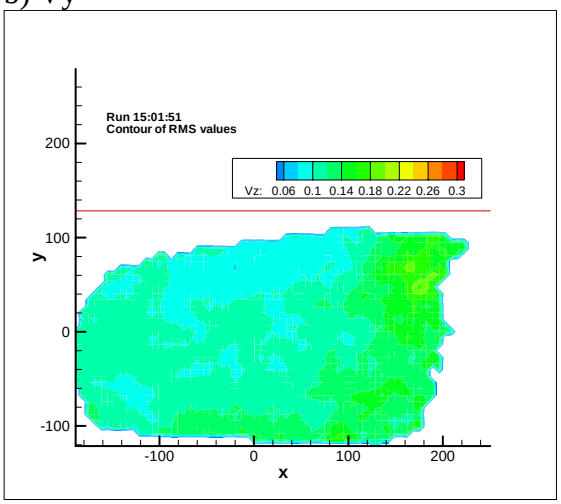

c) Vz

Figure 28, Run 15:01:51, Contours of RMS velocity component

Contours of RMS value for each velocity component over Run 15:01:51 for the complete sequence of time steps are shown in Figures 28(a) to 28(c). These figures show that the *x*, *y* and *z* components have similar values of RMS flow component, especially in the centre of the measurement window and the magnitude of the RMS value is mostly between 0.10 and 0.14, for an undisturbed flow speed of 0.5 m/s. The only exception is the very top right hand corner for the *x* velocity component, and this region is calculated from a smaller number of valid vectors.

The RMS values for the individual windows were combined using the same approach as the one used for the flow vectors. RMS values for each velocity component were placed on a common grid and points within the PIV mesh where no vectors were calculated were removed. The combined data were plotted as contours and interpolated on the same grid used for the velocity components. The resulting values are shown in Figures 29 to 34.

RMS values for the upstream location at midships are shown in Figures 29 and 30, for flow speeds of 0.5 and 1.0 m/s respectively. The highest turbulence was observed close to the hull and close to the free surface.

The downstream location with no fin is shown in Figures 31 and 32 for flow speeds of 0.5 m/s and 1.0 m/s. The highest areas of turbulence are close to the downstream bilge. In this measurement area the free surface had less effect on the unsteadiness in the flow.

Figures 33 and 34 show the RMS values for the case when the fin was fitted. The area of the highest turbulence extended the full depth of the measurement area and was in the same location as the vortex caused by the fin. A major effect of the fin was to increase the amount of turbulence in the flow.

In all cases, the level of turbulence does not change significantly between velocity components.

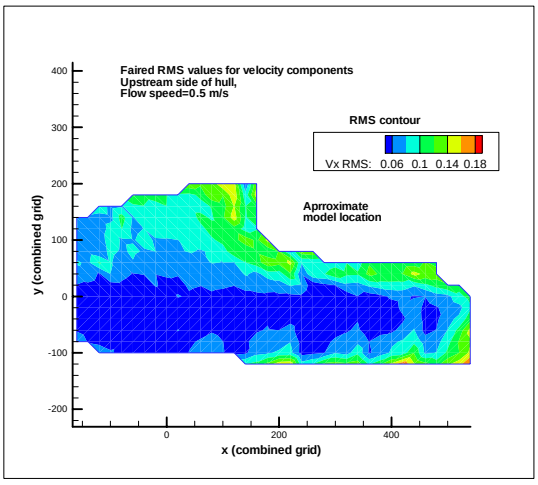

a) Vx

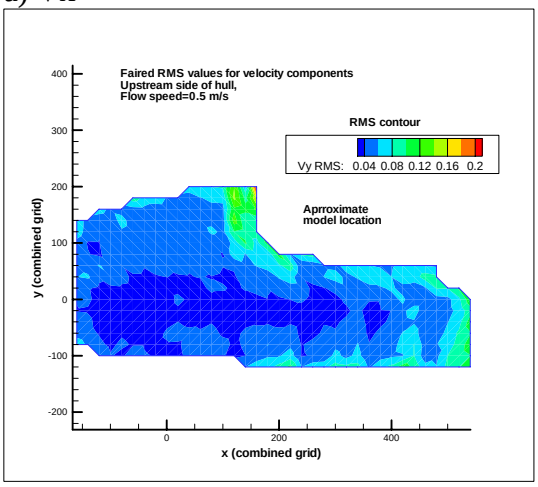

b) Vy

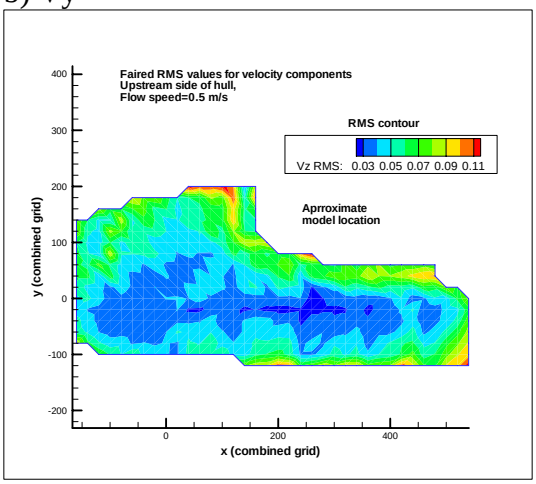

c) Vz

Figure 29, Contours of RMS for flow component, Upstream, 0.5 m/s

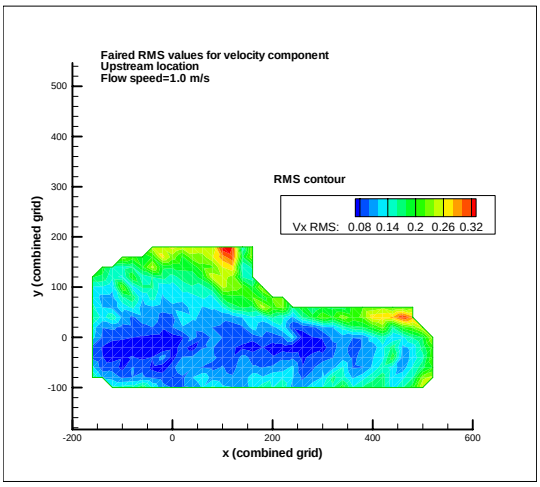

a) Vx

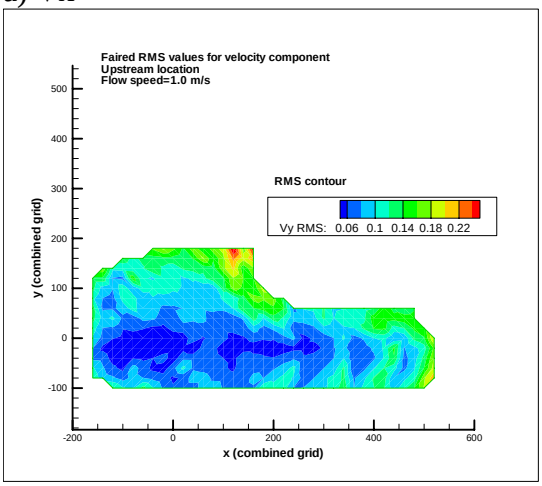

b) Vy

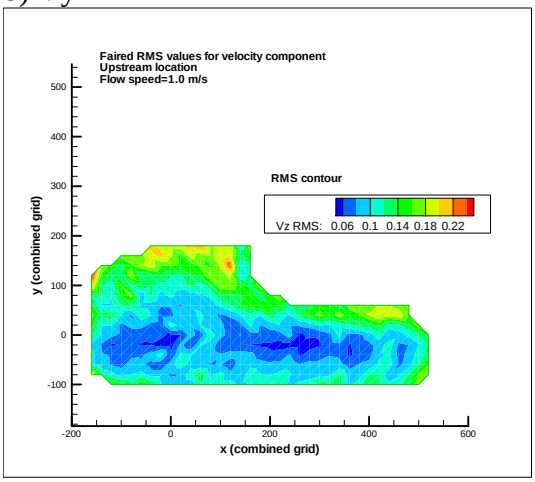

c) Vz

Figure 30, Contours of RMS for flow component, Upstream, 1.0 m/s

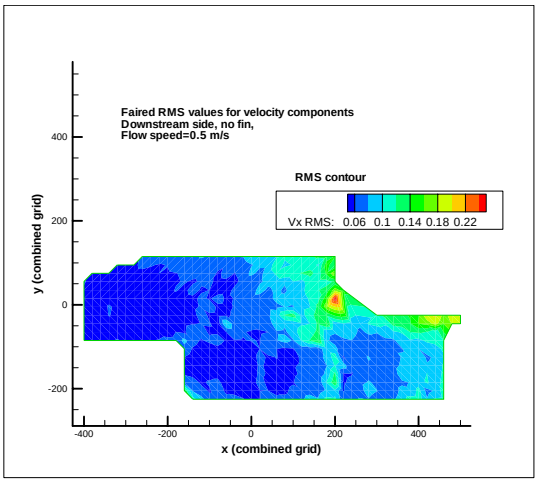

a) Vx

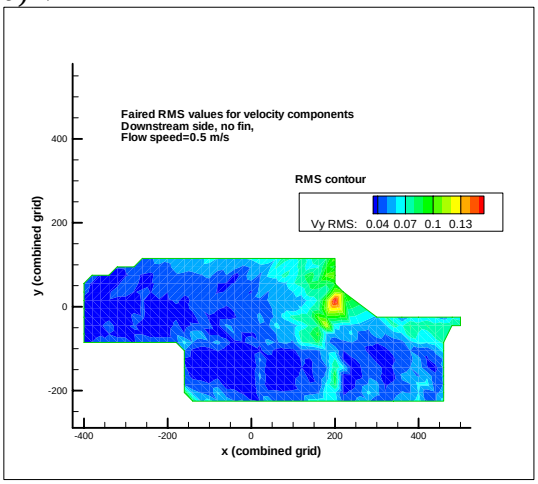

b) Vy

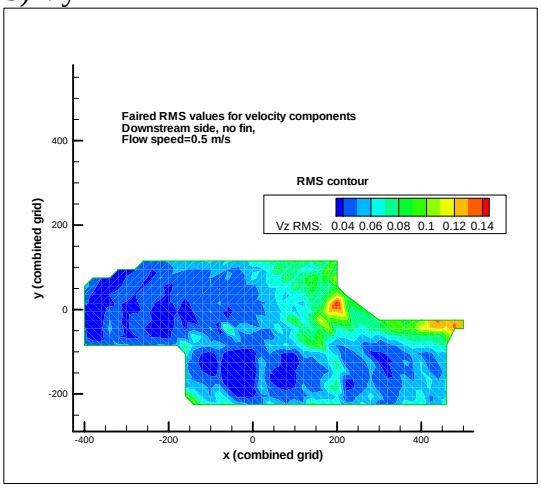

c) Vz

Figure 31, Contours of RMS for flow component, Downstream, no fin, 0.5 m/s

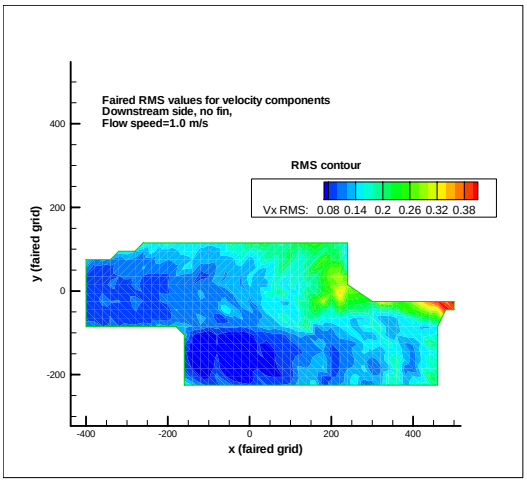

a) Vx

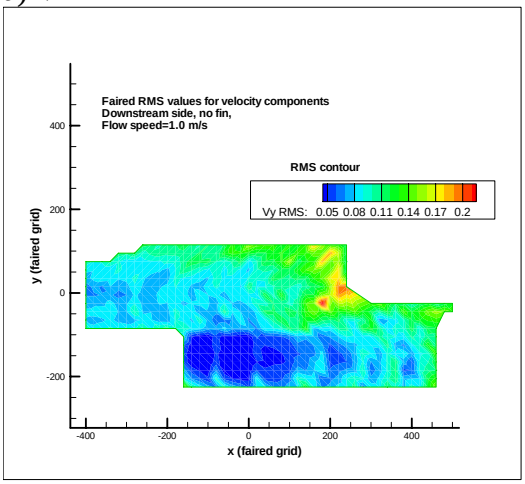

b) Vy

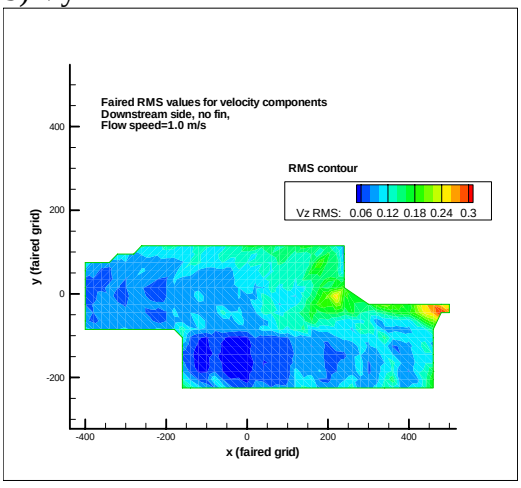

c) Vz

Figure 32, Contours of RMS for flow component, Downstream, no fin, 1.0 m/s

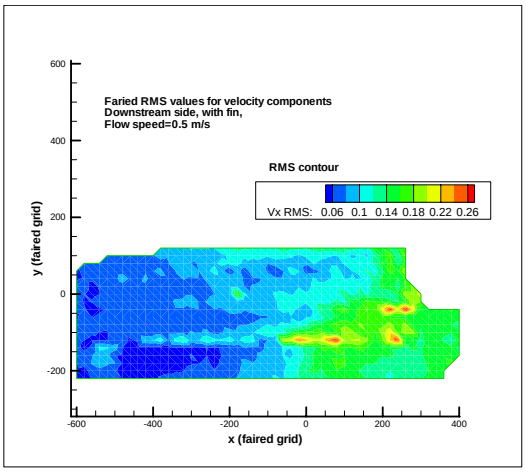

a) Vx

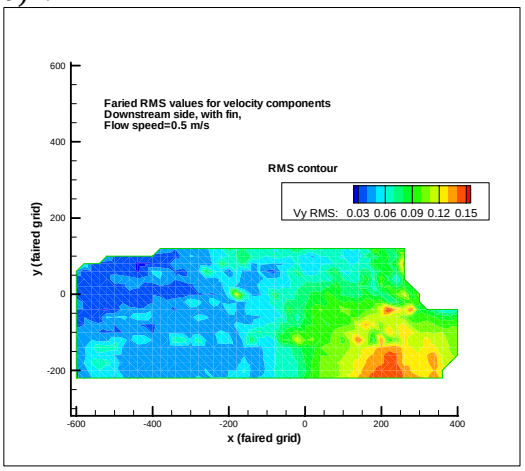

b) Vy

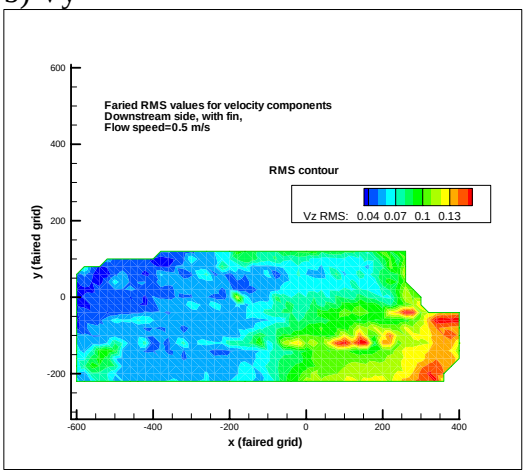

c) Vz

Figure 33, Contours of RMS for flow component, Downstream, with fin, 0.5 m/s

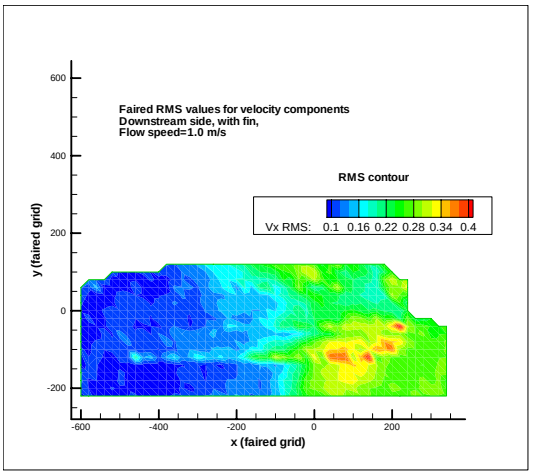

a) Vx

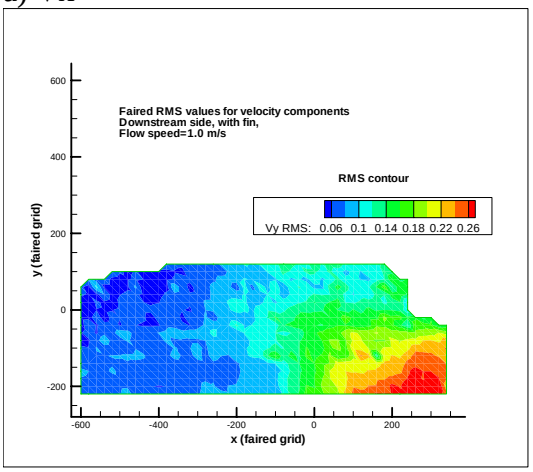

b) Vy

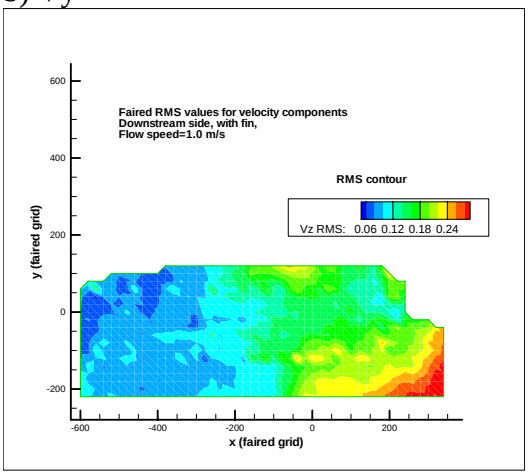

c) Vz

Figure 34, Contours of RMS for flow component, Downstream, with fin, 1.0 m/s

7.0 RECOMMENDATIONS FOR FURTHER WORK

The three-dimensional calibration of the measurement space using the purpose made stepped plate is very efficient. However, when examining the flow around a specific geometry, there needs to be an accurate method for locating the measurement space in relation to the geometry. The test plan developed using the IOT ice tank addressed the need to overlap multiple windows, but in the detailed analysis it would have been helpful to have a more accurate method for locating the model hull within the measurement plane. One method of doing this would have been to have had more reference points on the model, and then applying the calibration functions to these known points. In some locations, this could be done with the set-up used, because the chine at the bilge was clearly identifiable, but in other locations there were no reference points. Fortunately the edge of the model could be located from the vector patterns when all the windows were combined.

The seeding system would benefit from further refinement. The flow pattern around the tug at a yaw angle of 45 degrees was very complex, with high flow gradients and flow from the underside of the hull mixing with flow coming along the downstream side of the hull. All of the results were obtained with a single seeding rake, but the location of the rake relative to the model was moved for each measurement location. A refinement would have been to have two separate seeding rakes, so that different regions of the flow could be seeded at the same time.

8.0 CONCLUSIONS

Particle Image Velocimetry was successfully used to determine the flow velocities around an escort tug with a typical operating yaw angle of 45 degrees. One measurement direction was used, which was a plane normal to the direction of the undisturbed flow, which intersected with the tug's hull at midships. Measurements were made on the upstream and downstream sides of the tug. The total measurement area required to define the flow patterns around the hull was much larger than a single PIV measurement window (approximately 400 mm by 250 mm). In order to extend the measurement area beyond the singe window, the model was moved relative to the PIV system, by less than the dimensions of the window. As a result, the same area, relative to the model was seen in at least three measurement windows. The flow vectors from multiple views of the same location were averaged to obtain flow vectors over the complete measurement space.

Detailed measurements of the flow velocities around an escort tug model, operating at 45 degree of yaw is a hydrodynamic condition that has not been studied before. The key flow features identified were:

1) The separation of the incoming flow on the upstream side of the hull at the corner of the bilge and the reverse flow under the hull.

2) The formation of a vortex on the downstream side of the hull, which extended between the bottom of the hull and the waterline for the tug without the fin.

3) The formation of a large vortex on the downstream side of the hull when the fin was fitted. For a section at midships, the core of the vortex was located at approximately the mid-depth of the fin and the maximum beam of the model. This vortex changes the flow patterns close to the surface, and the smaller vortex seen when the fin was absent is not present at all.

The speeds for which the experiments were carried out covered the typical operating speeds of a tug, using Froude scaling. The direction of the flow vectors relative to the hull changed very little with the speed of the undisturbed flow, although the magnitude of the velocity components changed with the magnitude of the undisturbed flow.

Even though the flow around the tug model was turbulent, the long-term average flow vectors were stable. This was determined by using the longest practical time sequence of 100 image pairs, repeating measurements for given flow speeds and window locations, and overlapping measurement windows so that at least three views were obtained of key flow features.

9.0 ACKNOWLEDGEMENTS

I wish to thank the following people. Professor Neil Bose, Canada Research Chair in Offshore and Underwater Vehicles Design at Memorial University, is thanked for his continuing support and encouragement of our efforts to understand PIV and develop it into a practical experiment technique for ocean engineering and naval architecture research. Ms. Jie Xu is thanked for her leadership, continuous dedication and attention to detail that is necessary for making successful PIV experiments. Mr. Jim Gosse, Laboratory Technician in the Fluids Laboratory at Memorial University, is thanked for all his help setting up and carrying out the experiments in the OERC Towing Tank at MUN. Finally, I wish to thank the staff at IOT for preparing the model for testing and assisting with the many tasks required during the experiments at IOT.

10.0 REFERENCES

Allan R. G. & Molyneux, W. D. 2004 ‘Escort Tug Design Alternatives and a Comparison of Their Hydrodynamic Performance’, Paper A11, Maritime Technology Conference and Expo, S.N.A.M.E. Washington, D. C. September 30th to October 1st.

LaVision Inc. 2005 ‘DaVis Flowmaster Software Manual for DaVis 7.1’.

Molyneux, W. D. 2003 ‘Steering and Braking Force Predictions for a Z-Drive Tractor Tug’, NRC/IOT TR-2003-26.

Molyneux, W. D. 2005 ‘Plan for Particle Image Velocimetry Experiments of Flow Around a Model of an Escort Tug’, IOT/NRC, TR-2005-15.

Molyneux, W. D., and Xu, J. 2005 ‘Particle Image Velocimetry Experiments to Measure Flow Around and Escort Tug’, IOT/NRC, TR-2005-10.

Molyneux, W. D. 2006 ‘Description of the Stereoscopic Particle Image Velocimetry System Used by Memorial University of Newfoundland’, IOT/NRC, TR-2006-12.

Van den Braembussche, R. A. (editor) 2001 ‘*Measurement Techniques in Fluid Dynamics*’, Von Karman Institute for Fluid Dynamics, 2nd Revised Edition.

Wavemetrics Inc. 2004 ‘Igor Pro Version 5 Users Guide’.

APPENDIX 1

PARTICLE IMAGE VELOCIMETRY MEASUREMENTS FOR FLOW AROUND AN ESCORT TUG MODEL

TEST LOG

Table 1: Upstream side, no fin

Test date	Time	δt, μs	Speed, m/s	Beam to centreline, mm		borescope height, mm	x correction mm	y correction mm	# frames	Threshold	Notes
				laser	model						
30-Jan-06	14:20:08	1000	0.50	300	0	0	0	0	100	25	
	14:37:15	1000	0.50	300	0	0	0	0	100	25	
	14:44:17	1000	0.50	300	0	0	0	0	100	25	
	14:49:19	500	1.00	300	0	0	0	0	100	25	
	14:52:51	500	1.00	300	0	0	0	0	100	25	
30-Jan-06	15:03:22	1000	0.50	200	0	0	100	0	100	25	
	15:11:44	1000	0.50	200	0	0	100	0	100	25	
	15:18:06	500	1.00	200	0	0	100	0	100	25	Not used
	15:22:42	500	1.00	200	0	0	100	0	100	25	Not used
30-Jan-06	15:35:09	1000	0.50	200	0	0	100	0	100	25	Not used
	15:38:59	1000	0.50	200	0	0	100	0	100	25	Not used
	15:42:33	1000	0.50	200	0	0	100	0	100	25	Not used
	15:47:13	1000	0.50	200	0	0	100	0	100	25	Not used
	15:53:43	1000	0.50	200	0	0	100	0	100	25	Not used

Table 1 continued: Upstream side, no fin

Test date	Time	δt, μs	Speed, m/s	Beam to centreline, mm laser	model	borescope height, mm	x correction mm	y correction mm	# frames	Threshold	Notes
31-Jan-06	9:28:44	1000	0.50	200	0	0	100	0	100	25	
	9:33:31	1000	0.50	200	0	0	100	0	100	25	
	9:37:50	500	1.00	200	0	0	100	0	100	25	
	9:43:55	500	1.00	200	0	0	100	0	100	25	
	9:48:32	500	1.00	200	0	0	100	0	100	25	
31-Jan-06	10:01:01	1000	0.50	100	0	0	200	0	100	25	
	10:06:57	1000	0.50	100	0	0	200	0	100	25	
	10:14:27	500	1.00	100	0	0	200	0	100	25	
	10:19:16	500	1.00	100	0	0	200	0	100	25	
31-Jan-06	10:30:05	1000	0.50	0	0	0	300	0	100	25	
	10:34:41	1000	0.50	0	0	0	300	0	100	25	
	10:41:12	500	1.00	0	0	0	300	0	100	25	
	10:45:37	500	1.00	0	0	0	300	0	100	25	
31-Jan-06	11:09:34	1000	0.50	300	0	100	0	100	100	25	
	11:12:51	1000	0.50	300	0	100	0	100	100	25	
	11:24:20	1000	0.50	300	0	100	0	100	100	25	
	11:28:55	500	1.00	300	0	100	0	100	100	25	
	11:33:48	500	1.00	300	0	100	0	100	100	25	
	11:38:32	1000	0.50	300	0	100	0	100	100	25	
	11:41:00	1000	0.50	300	0	100	0	100	100	25	
	11:46:18	500	1.00	300	0	100	0	100	100	25	
	11:50:10	500	1.00	300	0	100	0	100	100	25	

Table 2, Downstream side, no fin

Test date	Time	δt, μs	Speed, m/s	Beam to centreline, mm		borescope	x correction	y correction	# frames	threshold
				laser	model	height, mm	mm	mm		
26-Jan-06	11:23:52	1000	0.5	100	0	-130	300	-130	100	25
	11:26:53	1000	0.5	100	0	-130	300	-130	100	25
	11:29:33	500	1.0	100	0	-130	300	-130	100	25
	11:33:43	500	1.0	100	0	-130	300	-130	100	25
	11:42:02	500	1.0	100	0	-130	300	-130	100	25
26-Jan-06	11:54:39	1000	0.5	200	0	-130	200	-130	100	25
	11:59:19	1000	0.5	200	0	-130	200	-130	100	25
	12:03:24	1000	0.5	200	0	-130	200	-130	100	25
	12:17:34	500	1.0	200	0	-130	200	-130	100	25
	12:23:20	500	1.0	200	0	-130	200	-130	100	25
	12:30:24	500	1.0	200	0	-130	200	-130	100	25
	12:36:23	500	1.0	200	0	-130	200	-130	100	25
26-Jan-06	13:54:46	1000	0.5	300	0	-130	100	-130	100	25
	14:04:17	1000	0.5	300	0	-130	100	-130	100	25
	14:08:55	500	1.0	300	0	-130	100	-130	100	25
	14:12:19	500	1.0	300	0	-130	100	-130	100	25
26-Jan-06	14:20:34	1000	0.5	400	0	-130	0	-130	100	25
	14:27:11	1000	0.5	400	0	-130	0	-130	100	25
	14:30:57	500	0.5	400	0	-130	0	-130	100	25
	14:34:56	500	1.0	400	0	-130	0	-130	100	25
	14:38:19	500	1.0	400	0	-130	0	-130	100	25

Table 2 continued, Downstream side, no fin

Test date	Time	δt, μs	Speed, m/s	Beam to centreline, mm		borescope height, mm	x correction mm	y correction mm	# frames	threshold
				laser	model					
27-Jan-06	9:59:19	1500	0.5	400	100	20	-100	0	100	25
	10:08:39	1500	0.5	400	100	20	-100	0	100	25
	10:15:31	700	1.0	400	100	20	-100	0	100	25
	10:24:33	700	1.0	400	100	20	-100	0	100	25
	10:28:38	700	1.0	400	100	20	-100	0	100	25
27-Jan-06	10:38:17	1500	0.5	400	200	20	-200	0	100	25
	10:48:40	1500	0.5	400	200	20	-200	0	100	25
	10:51:54	700	1.0	400	200	20	-200	0	100	25
	10:56:20	700	1.0	400	200	20	-200	0	100	25
27-Jan-06	11:11:08	1500	0.5	400	300	20	-300	0	100	25
	11:16:34	1500	0.5	400	300	20	-300	0	100	25
	11:22:25	700	1.0	400	300	20	-300	0	100	25
	11:26:45	700	1.0	400	300	20	-300	0	100	25
27-Jan-06	15:12:48	500	0.5	400	0	20	0	0	100	25
	15:15:16	1000	0.5	400	0	20	0	0	100	25
	15:17:59	500	1.0	400	0	20	0	0	100	25
	15:20:52	500	1.0	400	0	20	0	0	100	25
	15:27:18	1000	0.5	400	0	20	0	0	100	25
	15:30:41	1000	0.5	400	0	20	0	0	100	25
	15:33:32	1000	0.5	400	0	20	0	0	100	25
	15:39:09	500	1.0	400	0	20	0	0	100	25
	15:42:35	500	1.0	400	0	20	0	0	100	25
	15:48:13	500	1.0	400	0	20	0	0	100	25

Table 3, Downstream side, with fin

Test date	Time	δt, μs	Speed, m/s	Beam to centreline, mm		borescope height, mm	x correction mm	y correction mm	# frames	Threshold	Notes
				laser	model						
18-Jan-06	15:29:35	1000	0.5	400	0	0	0	0	50	12	
	15:35:09	1000	1.0	400	0	0	0	0	50	12	
	15:48:14	2000	0.5	400	0	0	0	0	50	12	
	15:51:13	1000	1.0	400	0	0	0	0	50	12	
19-Jan-06	10:00:15	2000	0.5	400	100	0	-100	0	50	12	Not used
	10:06:41	2000	1.0	400	100	0	-100	0	50	12	Not used
	10:13:30	1000	1.0	400	100	0	-100	0	50	12	Not used
	10:26:17	2000	0.5	400	100	0	-100	0	50	12	
	10:29:36	2000	0.5	400	100	0	-100	0	50	12	
	10:33:14	1000	0.5	400	100	0	-100	0	50	12	
	10:39:31	1000	1.0	400	100	0	-100	0	50	12	
	10:42:39	1000	1.0	400	100	0	-100	0	50	12	
19-Jan-06	10:57:10	2000	0.5	400	200	0	-200	0	50	12	
	11:01:16	2000	0.5	400	200	0	-200	0	50	12	
	11:07:01	2000	0.5	400	200	0	-200	0	50	12	
	11:11:05	1000	1.0	400	200	0	-200	0	50	12	
	11:18:52	2000	0.5	400	200	0	-200	0	50	12	
	11:21:44	1000	1.0	400	200	0	-200	0	50	12	
	11:27:18	1000	1.0	400	200	0	-200	0	50	12	
19-Jan-06	11:40:33	2000	0.5	400	300	0	-300	0	50	12	
	12:04:06	2000	0.5	400	300	0	-300	0	50	12	
	12:10:37	2000	0.5	400	300	0	-300	0	50	12	
	12:13:36	1000	1.0	400	300	0	-300	0	50	12	
	12:18:04	1000	1.0	400	300	0	-300	0	50	12	

Table 3 continued, Downstream side, with fin

Test date	Time	δt, μs	Speed, m/s	Beam to centreline, mm laser	Beam to centreline, mm model	borescope height, mm	x correction mm	y correction mm	# frames	Threshold	Notes
19-Jan-06	13:43:16	2000	0.5	400	400	0	-400	0	50	12	
	13:51:39	2000	0.5	400	400	0	-400	0	50	12	
	13:56:21	2000	0.5	400	400	0	-400	0	50	12	
	13:59:51	2000	1.0	400	400	0	-400	0	50	12	Not used
	14:07:31	1000	1.0	400	400	0	-400	0	50	12	
	14:11:38	1000	1.0	400	400	0	-400	0	50	12	
	14:22:12	2000	0.5	400	500	0	-500	0	50	12	
	14:28:44	2000	0.5	400	500	0	-500	0	50	12	
	14:32:14	2000	0.5	400	500	0	-500	0	50	12	
	14:34:24	1000	1.0	400	500	0	-500	0	50	12	
	14:36:50	1000	1.0	400	500	0	-500	0	50	12	
24-Jan-06	14:40:28	1500	0.5	400	0	-130	0	-130	100	25	Not used
	14:46:39	1500	0.5	400	0	-130	0	-130	100	25	Not used
	14:53:32	700	1.0	400	0	-130	0	-130	100	25	
	15:02:23	700	1.0	400	0	-130	0	-130	100	25	
	15:12:52	700	1.0	400	0	-130	0	-130	100	25	Not used
	15:21:00	700	1.0	400	0	-130	0	-130	100	25	Not used
24-Jan-06	15:35:21	1500	0.5	400	100	-130	-100	-130	100	25	Not used
	15:44:58	1500	0.5	400	100	-130	-100	-130	100	25	Not used
	15:47:46	1500	0.5	400	100	-130	-100	-130	100	25	
	15:50:58	700	1.0	400	100	-130	-100	-130	100	25	
	15:54:59	700	1.0	400	100	-130	-100	-130	100	25	Not used

Table 3 continued, Downstream side, with fin

Test date	Time	δt, μs	Speed, m/s	Beam to centreline, mm		borescope height, mm	x correction mm	y correction mm	# frames	Threshold	Notes
				laser	model						
25-Jan-06	9:51:34	1500	0.5	400	200	-130	-200	-130	100	25	
	9:56:45	1500	0.5	400	200	-130	-200	-130	100	25	
	10:01:44	1500	0.5	400	200	-130	-200	-130	100	25	
	10:04:53	700	1.0	400	200	-130	-200	-130	100	25	
	10:10:36	1000	1.0	400	200	-130	-200	-130	100	25	
25-Jan-06	10:26:00	1500	0.5	400	300	-130	-300	-130	100	25	Not used
	10:29:56	1500	0.5	400	300	-130	-300	-130	100	25	Not used
	10:33:20	1000	1.0	400	300	-130	-300	-130	100	25	Not used
	10:41:12	1500	0.5	400	300	-130	-300	-130	100	25	
	10:45:03	1500	0.5	400	300	-130	-300	-130	100	25	
	10:47:24	1500	0.5	400	300	-130	-300	-130	100	25	
	10:50:43	700	1.0	400	300	-130	-300	-130	100	25	
	10:54:50	700	1.0	400	300	-130	-300	-130	100	25	
25-Jan-06	11:03:55	1500	0.5	400	400	-130	-400	-130	100	25	
	11:07:06	1500	0.5	400	400	-130	-400	-130	100	25	
	11:11:31	700	0.5	400	400	-130	-400	-130	100	25	
	11:14:38	700	1.0	400	400	-130	-400	-130	100	25	
	11:23:05	700	1.0	400	400	-130	-400	-130	100	25	
	11:27:01	1500	1.0	400	400	-130	-400	-130	100	25	

Table 3 continued, Downstream side, with fin

Test date	Time	δt, μs	Speed, m/s	Beam to centreline, mm		borescope	x correction	y correction	# frames	threshold	Notes
25-Jan-06	11:38:00	1500	0.5	400	500	-130	-500	-130	100	25	
	11:42:01	1500	0.5	400	500	-130	-500	-130	100	25	
	11:45:24	700	1.0	400	500	-130	-500	-130	100	25	
	11:51:04	500	1.0	400	500	-130	-500	-130	100	25	Not used
	11:57:13	700	1.0	400	500	-130	-500	-130	100	25	Not used
	12:01:25	1000	1.0	400	500	-130	-500	-130	100	25	
25-Jan-06	14:25:16	1500	0.5	300	0	-130	100	-130	100	25	Not used
	14:29:41	1000	0.5	300	0	-130	100	-130	100	25	Not used
	14:29:53	1000	0.5	300	0	-130	100	-130	100	25	Not used
	14:32:41	800	0.5	300	0	-130	100	-130	100	25	
	14:35:52	1000	0.5	300	0	-130	100	-130	100	25	
	14:40:08	700	1.0	300	0	-130	100	-130	100	25	
	14:45:21	700	1.0	300	0	-130	100	-130	100	25	
25-Jan-06	15:01:51	1000	0.5	200	0	-130	200	-130	100	25	
	15:08:14	1500	0.5	200	0	-130	200	-130	100	25	
	15:12:33	1500	0.5	200	0	-130	200	-130	100	25	
	15:16:46	700	1.0	200	0	-130	200	-130	100	25	
	15:22:43	700	1.0	200	0	-130	200	-130	100	25	
25-Jan-06	15:37:17	1500	0.5	100	0	-130	300	-130	100	25	Not used
	15:59:53	1500	0.5	100	0	-130	300	-130	100	25	
	16:09:04	700	1.0	100	0	-130	300	-130	100	25	
	16:15:34	700	1.0	100	0	-130	300	-130	100	25	
	16:41:06	1500	0.5	100	0	-130	300	-130	100	25	Not used